Fire behaviour of reinforced concrete slabs under combined biaxial in-plane and out-of-plane loads

Citation for published version:
Wang, Y, Bisby, LA, Wang, T, Yuan, G & Baharudin, E 2018, 'Fire behaviour of reinforced concrete slabs under combined biaxial in-plane and out-of-plane loads', *Fire Safety Journal*, vol. 96, pp. 27-45.
https://doi.org/10.1016/j.firesaf.2017.12.004

Digital Object Identifier (DOI):
10.1016/j.firesaf.2017.12.004

Link:
Link to publication record in Edinburgh Research Explorer

Document Version:
Peer reviewed version

Published In:
Fire Safety Journal

Fire behaviour of reinforced concrete slabs under combined bi-axial in-plane and out-of-plane loads

Yong Wang [a,b]*, Luke A Bisby [c], Teng-yan Wang [a], Guanglin Yuan [a], Emran Baharudin [c]

(*[a] State Key Laboratory for Geomechanics and Deep Underground Engineering, China University of Mining and Technology, Xuzhou, Jiangsu 221116, China;*

[b] Jiangsu Collaborative Innovation Center for Building Energy Saving and Construction Technology, Xuzhou, Jiangsu 221116, China;

[c] School of Engineering, University of Edinburgh, Edinburgh EH9 3JN, UK)

Abstract: To better understand the fire behaviour of in-plane restrained reinforced concrete slabs, this paper presents six fire tests on two-way spanning concrete slabs under compressive bi-axial in-plane and flexural out-of-plane loads. The data presented include furnace temperatures, temperature distributions, vertical and horizontal deflections, restraint forces, crack patterns, and characterisation of spalling of the six slabs during both heating and cooling phases. Comparison of the results indicates that bi-axial in-plane loads may have a negative effect on the vertical and horizontal deflection trends of the restrained slabs in fire. In addition, snap though behaviour and subsequent severe reversals of deflection trends were observed for the first time in concrete slabs with sustained bi-axial in-plane restraint during heating and cooling stages. Fire behaviour of the restrained slabs were considerably different from those of the simply supported slabs, and thus the effect of uniaxial or bi-axial in-plane restraints on the failure mode should be considered to establish reasonable failure criteria for these slabs. In addition, it is suggested that the corners of the in-plane restrained slabs should be reinforced by arranging the whole span top steels along two directions since the corners easily fracture with large diagonal cracks during fire tests.

Keywords: reinforced concrete slabs; fire test; bi-axial restraint; deflection; crack; snap through

1. Introduction

In recent years, a number of experimental studies for investigating the fire behavior of reinforced concrete slabs have been conducted [1-7]. In 2013 and 2015, fire tests in one steel-framed building [5-7] indicated that reinforced concrete floor slabs at larger deflections played a key role in enhancing the fire resistance of the steel-framed building due to the tensile membrane action. It is also acknowledged that the behavior of reinforced concrete slabs in fire is affected by the slabs' support conditions. In other words, the structural continuity and the interactions between adjacent elements in a whole structure have significant effect on the structural fire behaviour which is different from that observed in isolated member tests. The deformations and cracking patterns of the floor are highly dependent on the locations of the fire compartments within the buildings, i.e., the boundary restraint conditions. For instance, the clear plateau was observed in the mid-span deflection of heated panels in the building, and the greater boundary restraint resulted in a longer plateau duration. In addition, the top surface cracks of the interior panel were clearly different from those of the corner panels due to the different in-plane restraint and rotation restraint [5-7].

In fact, from the 1960s, the effects of restraint on concrete slabs in fire have been investigated by many researchers through fire tests [8-11], numerical analysis [12-14] and theoretical methods [15-17]. However, a review of literature shows that there are some obvious controversies on the effect of the restraint on the fire behavior of concrete slabs, as discussed in [18]. The majority of fire tests on reinforced concrete slabs have been tested under simply supported conditions. Hence, further experimental research on concrete slabs in fire with well-controlled axial restraint forces is needed. This approach allows the research to concentrate on the most important phenomena in question [19].

In 2016, Wang et.al [18] conducted a series of fire tests, which included four full-scale reinforced concrete square slabs (Slabs S1 to S4), under combined uniaxial in-plane and flexural out-of-plane loading, and with vertical restraint at the four corners of the slabs. This prior research was focused on the quantitative relationship between horizontal restraint forces and deformations, cracking patterns, and spalling of the slabs in fire. The test results indicated that: (1) the mid-span vertical and horizontal deflections of the slabs with combined horizontal uniaxial in-plane (1MPa or 2MPa) and vertical out-of-plane forces (2kPa) are larger than those of the slabs without uniaxial in-plane restraint forces, with the average increased deflection ratio of 40% and 53.3% at 180min, respectively; (2) cracks parallel to the in-plane restraint force could be observed in the uniaxial restrained slabs, which may be due to the Poisson's effect. In addition, for the restrained slabs, the reduction in the number of cracks can be achieved efficiently by increasing the reinforcement ratio; and (3) restrained slabs with large uniaxial in-plane forces tend to fail by integrity failure resulting from full-depth cracks in the slabs.

As reported in [18], the previous fire tests were mainly conducted on square slabs with uniaxial in-plane restraint. As a part of a series of tests on conventional concrete slabs, the authors continued to investigate the effect of bi-axial restraint forces on the fire behavior of four rectangular slabs (Slabs R1 to R4) and two additional square slabs (Slabs S5 and S6). The test results were compared with those published in the literature, and provide data that can be used to verify numerical or theoretical models and provide an empirical basis for more rational design methodologies for restrained concrete slabs in fire.

2. Test programme

2.1 Test furnace

A furnace was specially designed and constructed to heat six concrete slabs, as shown in Figs. 1(a) and 1(b). The four furnace side walls were constructed from refractory bricks and were composed of an outer furnace wall (370mm deep) and mineral wool (50mm deep). The rectangular slabs, the dimensions of the furnace were 3900×3270×1500mm. One furnace wall (dash lines in Fig. 1(a)) was built in the same furnace to conduct two fire tests of square slabs, and the dimensions of the furnace in this case were 3270×3270×1500mm. The test program of the square slabs under bi-axial restraint forces was similar to those of Slabs S1 to S4 tested under uniaxial restraint forces [18], and thus a detailed description of these two tests is avoided in the current paper.

2.2 Concrete slabs

In the current paper, six slabs were simply supported on four edges and subjected to various combinations of horizontal uniaxial or bi-axial in-plane and vertical out-of-plane loads. Slab R1 was tested under vertical out-of-plane load only, for the purposes of comparison, and Slab R2 was tested under uniaxial in-plane load applied on its short edges. The other four slabs (Slabs R3, R4, S5 and S6) were tested under bi-axial in-plane loads, as outlined in Table 1. Each slab was vertically clamped at all four corners. The slabs were identical in terms of nominal concrete strength, steel reinforcement, and concrete cover depth.

All six slabs were cast on the same day (same batch) and were stored indoors in the laboratory to cure. Due to the testing condition, the temperature and relative humidity were not controlled in the laboratory. The age of the concrete at the time of testing was: Slab R1 = 156 days; Slab R2 = 171 days; Slab R3 = 193 days; Slab R4 = 200 days, Slab S5 = 230 days and Slab S6 = 243 days. Commercial normal weight concrete (siliceous aggregate) with the specified compressive cube strength of 30 MPa at 28 days was used for the slabs. Concrete tests and moisture content were performed at each fire test. The actual average compressive strength of concrete at the time of testing was 34 MPa, with the standard deviation of 3.8. In addition, the average moisture content measured by the cubic specimens (100mm×100mm×100mm) was 7.4%, with the standard deviation of 0.6%. For each slab, hot-rolled reinforcing bars of 8 mm diameter were arranged at 200 mm spacing along the two directions, with the clear concrete cover of 15 mm. To be conservative, reinforcement was only placed at the bottom of the slabs. The tested average yield strength and ultimate strength of the reinforcing steel were 485MPa and 577 MPa, respectively.

2.3 Instrumentation

Two Type-K (2mm diameter) thermocouples, i.e., F-1 and F-2, were used to measure the furnace temperatures during each fire test. For each test, nine thermocouple trees (T1 to T9) were used to measure the temperature of each slab, as shown in Fig. 2(a). Each thermocouple tree consisted of 6 Type-K (0.5mm diameter) thermocouples distributed vertically to measure the concrete temperature, and the distances between these (points T-1 to T-6) were 20mm on center. Two thermocouples (points R-1 and R-2) were placed at the mid-depth of the bottom steel bars, as shown in Fig. 2(b).

Fig. 3 shows the position of vertical and horizontal displacement transducers (with limit travel ranging from 10-500mm). Eight linear variable differential transformer LVDT's (V1-V8) were placed to measure the vertical deflections of the slab, while its horizontal deflections were measured by two LVDT’s (H-1 and H-2), respectively.

2.4 Test setup and procedure

The four simply-supported edges of each slab were supported by steel balls and rollers on the furnace walls, in accordance with the Standard of Concrete Testing Method of China [20]. A uniformly distributed load 2.0 kN/m^2 (using sandbags) was applied on the top of each slab to simulate superimposed loads, according to the Chinese load code for the design of building structures [21]. Additional details are given in [18].

As shown in Fig. 4(a), the in-plane loads were applied by an independent loading frame. Three loading jacks in each direction were used to simulate uniform uniaxial in-plane loads for the restrained rectangular or square slabs. The in-plane load was applied to the slab by steel knife edges attached to the rams of six 500kN hydraulic jacks along two edges of the slab. At the other two edges of the slab, six knife edges were also bolted to the closed frame to provide the reaction for the applied in-plane load, as shown in Fig. 4(b). During each test, each corner was held down by a steel beam, and the restraint forces in the four corners were measured by four pressure transducers (P-1 to P-4). Each jack load was measured by a pressure transducer (i.e. P-5 to P-10). Full details of steel beams and steel supports are given in [18].

For each restrained slab, the out-of-plane load was first applied, and the in-plane load was then applied to a predetermined value (1MPa or 2MPa). The applied force was determined according to the full-scale testing results [10, 18], i.e., it was observed that the magnitude of average in-plane restraint stress was about 1MPa. The in-plane forces were intended to be kept as constant as possible during the tests. The main reason is that the constant restraint stress can be easily used to conduct the numerical analysis. As discussed above, this approach allows the research to concentrate on the effect of in-plane restraint on the fire behavior of two-way slabs. For Slab R2, the in-plane forces were applied only in the N-S direction, for Slabs R3, R4, S5 and S6, the in-plane forces were applied in the N-S and W-E directions, respectively. In addition, as the edges of the slab deflected up or down during testing, the in-plane loading frame also moved up or down accordingly.

3. Experimental results and discussions

This section discusses the experimental results for each slab, along with a brief explanation of the observed behaviours, including temperatures, deflections, and restraint forces during both heating and cooling phases; failure modes of six slabs are also presented. Finally, the test results are discussed in light of data reported in the literature, to better understand the effect of restraint on concrete slabs in fire.

3.1. Thermal response

3.1.1 Furnace temperature

The measured furnace temperatures with time during both the heating and cooling phases for all six slabs are shown in Figs. 5(a) through 5(f). For Slab S5, the power supply in the lab was suddenly interrupted 10min minutes into the test and all test data were lost. After 10min, the test was started again, and the furnace temperature at that time was about 180^{o}C.

As indicated in Figs. 5(a) through 5(f) the furnace temperatures deviated considerably from the ISO standard fire. In addition, because of higher moisture within the walls of the bespoke testing furnace, the gas temperatures recorded for the test of Slab R1 increased more slowly during the heating stage; this test was halted after 240min. For Slabs R2 to R4, S5 and S6, the test was halted after 180min, 190min, 180min, 73min and 180min, respectively. Note that, the shut-off time was mainly determined based on the failure criteria [26], including temperature failure criteria, deflection failure criterion and integrity criterion, as discuss later. As shown in Fig. 5(d), for Slab R4, due to malfunction of one of the two burners, the furnace temperature for Slab R4 decreased sharply at 120min. As shown in Fig. 5(e), for Slab S5, the test was terminated after 73min because multiple holes appeared in the slab and the fire passed through.

During the heating stage, the maximum recorded furnace temperatures for Slabs R1 to R4, S5 and S6 were 838^{o}C, 816^{o}C, 837^{o}C, 723^{o}C, 752^{o}C and 904 ^{o}C, respectively. Average furnace temperatures at the corresponding shut-off time were 829^{o}C, 809^{o}C, 833^{o}C, 559^{o}C, 750^{o}C and 888^{o}C, respectively, as shown in Tables 2 and 3. During the cooling stage, furnace temperatures decreased rapidly, and data recording finished after 400min, 300min, 300min, 300min, 160min and 300min for the six tests, respectively.

As reported in [18], the average furnace temperatures of four tests (Slabs S1 to S4) at 180 min were 827 ^{o}C, 800 ^{o}C, 918 ^{o}C and 837 ^{o}C, respectively, and then the furnace temperature decreased rapidly. The average furnace temperatures of Slabs R1 to R4, S5 and S6 tended to be lower than those of Slabs S1 to S4.

3.1.2 Temperature of the concrete slabs

(1) Concrete temperatures

Figs. 6(a)-6(f) show the temperature profiles along the cross sections at different locations of Slabs R1 to R4, S5 and S6. As expected, all six slabs had comparable temperature trends through the thickness with different temperature gradients due to the different furnace temperature curves followed. For instance, the temperatures on the bottom surfaces of the six slabs reached 633^{o}C (R1-T4-1), 616^{o}C (R2-T1-1), 674^{o}C (R3-T3-1), 380^{o}C (R4-T9-1), 616^{o}C (S5-T9-1) and 742 ^{o}C (S6-T4-1) at their corresponding shut-off times, respectively. Meanwhile, the temperatures on the top surface of six slabs were 249^{o}C (R1-T4-6), 148^{o}C (R2-T1-6), 184^{o}C (R3-T3-6), 142^{o}C (R4-T9-6), 98^{o}C (S5-T9-6) and 156^{o}C (S6-T4-6), respectively, and thus the differences were 384^{o}C, 468^{o}C, 490^{o}C, 238^{o}C, 518^{o}C and 586^{o}C, respectively. The temperature gradient of Slab R4 was the lowest due to the lowest furnace temperatures, and that of Slab S6 was the highest due to the highest furnace temperature. Note that, the temperature and gradients of the present slabs were relatively lower than those of Slabs S1 to S4 [18], and thus the lower temperature gradients resulted in lower mid-span deflections or deflection ratios.

In addition, the temperature-thickness curves of two slabs (Slabs S5 and S6) at different times were indicated in Figs.6 (g) and 6(h). The temperature gradient of Slab S5 was different from the normal temperature gradient [27], which led to its different fire behavior, especially the deflection and spalling, as discussed later.

Similar to the conclusions of [3-7], short temperature plateaus are observed in the thermocouple readings near to the unheated faces of the slabs. According to the concrete slab temperature failure criterion for insulation [22], i.e., an average temperature exceeding 140^{o}C or a maximum temperature measured by any one of the five thermocouples exceeding 180^{o}C, the standard fire resistance of six slabs by the Insulation Criterion can be determined as shown in Table 4.

(2) Rebar Temperatures

Figs. 7(a) through 7(f) illustrate the temperature development of reinforcing bars at different locations in the six slabs during testing. For each test, the measured temperatures at different points are similar during the initial heating stage. As the tests continued, however, temperature differences appeared at various positions due to their locations, water evaporation, and – importantly – concrete spalling. For instance, Fig. 7(a) shows that at 240min the temperatures in the bottom reinforcing bars of Slab R1 were 651^{o}C (T4-R-1) and 575^{o}C (T4-R-2), 623^{o}C (T5-R-1), 552^{o}C (T5-R-2), 585^{o}C (T6-R-1) and 453^{o}C (T6-R-2), respectively, with the average values at Points R-1 and R-2 of 620^{o}C and 527^{o}C, respectively. Similar conclusions can be drawn from the other five restrained slabs. As shown in Figs. 7(b)-7(f), at the corresponding shut-off time, average values of Point R-1 (R-2) were 495^{o}C (452^{o}C), 582^{o}C (515^{o}C), 362^{o}C (326^{o}C), 398 ^{o}C (289^{o}C) and 547 ^{o}C (519 ^{o}C) respectively. Clearly, the steel temperatures of Slabs R4 and S5 were lower due to the lower furnace temperature or short heating. In addition, for Slab S5, there was larger temperature difference on the reinforcements at different locations due to the most serious concrete spalling. For instance, as shown in Fig. 7(e), at the shut-off time, the temperatures at Points T4-R-1 and T5-R-2 were 480^{o}C and 253^{o}C, respectively. Finally, according to the steel failure criterion [22], i.e., the steel temperature exceeds 593^{o}C, and thus the prescriptive fire resistance of the six concrete slabs based on reinforcement temperature limits can be determined as indicated in Table 4.

3.2 Deflection response

This section discusses the vertical and horizontal deflections of six concrete slabs during the heating and cooling. For the vertical deflection, negative displacement is shown downward; while for the horizontal deflections, positive displacement indicates inward deflection (contraction).

3.2.1 Vertical deflections

1. Deflection versus time curves

(1) Effect of in-plane restraint forces

The measured vertical deflections during both the heating and cooling phases for Slabs R1 to R4, S5 and S6 are plotted against time, as shown in Figs. 8(a)-8(f). Different deflection trends are observed due to the differing thermal gradients, in-plane restraint forces, restraint types, and extent of concrete spalling. However, similar to the results observed for Slabs S1 to S4 [18], the mid-span deflections of the restrained slabs tend to be larger than those of the simply-supported slabs at later stages of the tests.

The comparison shows that in-plane restraint forces and concrete spalling affected the initial deflections (ratios) for Slabs R1 to R4. Even though the restraint slabs had higher furnace temperature and higher temperature gradient (Table 2 and Figs. 5(a)-5(d)), they had lower deflections or deflection ratios during the early stages. For instance, at 60min, the temperature gradient (133^{o}C) of Slab R1 was lower than those (265^{o}C, 316^{o}C and 149^{o}C) of Slabs R2 to R4. However，the mid-span deflection (27.5mm) and deflection ratio

(0.46mm/min) of the Slabs R1 was higher than the deflections (24.8mm, 17.2mm and 21.3mm) and deflection ratios (0.41mm/min, 0.29mm/min and 0.36mm/min) of Slabs R2 to R4. The reason is that the restraint forces produced compressive membrane action, which reduced the positive moments at the mid-span. The reduction of the positive moments at mid-span led to the slabs' lower deflection. On the other hand, the mid-span deflections and deflection ratios of Slabs R1 and R2 were larger than those of bi-axial restrained Slabs R3 and R4. This may be due to the serious spalling that occurred in Slabs R1 and R2 at the early stage. In contrast, Slabs R3 and R4 with bi-axial restraint showed little spalling at their bottom surfaces, as discussed later.

As the tests continued, the effect of the in-plane restraint forces on the deflections of the restrained rectangular slabs becomes evident, particularly at the later stages. For instance, at 180min, the mid-span deflections of the Slabs R1 to R4 were 58.5mm, 66.2mm and 70.6mm and 48.9mm, respectively. Compared with the mid-span deflection of Slab R1, the mid-span deflections of Slabs R2 and R3 increased by 13.2% and 20.7%, respectively. As discussed in [12, 18], this due to the P-δ effect generated from the in-plane restraint forces.

In addition, as reported in [18], the mid-span deflections of Slabs S1 to S4 were 76 mm, 120 mm, 100 mm and 101 mm at 180min, respectively. Due to higher concrete (steel) temperature and temperature gradient, these slabs had larger deflections. This comparison further implies that the furnace temperature is the main factor that determines the deflection of the restrained concrete slabs. In addition, it is interesting to note that there was a plateau of mid-span deflection of Slab R4 under bi-axial restraint between 120 min and 180 min due to the decreased furnace temperature (Fig.5 (d)). However, as reported in [18], the mid-span deflection of Slab S2 under uniaxial restraint always increased even though there was a furnace temperature plateau (about 60min). This is due to the fact that the rectangular Slab R4 behaved two-way action due to the bi-axial restraint, but the square Slab S2 under uniaxial restraint was essentially behaving in a one-way manner. For the bi-axial restraint, the compressive membrane action is the main load-carrying mechanism of the slab for this support condition [34]. For the uniaxial restraint slabs with larger deflection, the arch effect was lost, the compressive forces became detrimental to the slab as they increased the applied moments at mid-span and accelerated the deflection, i.e., P-δ effect [12]. Different cracking patterns in Slabs S2 and R4 also support this conclusion. For instance, the cracks within Slab S2 were mainly parallel to the in-plane force [18], but the cracks within Slab R4 developed across two whole spans, as discussed later. This shows that in-plane restraint types have important effects on the deflections of restrained slabs in fire.

At the corresponding shut-off time, the mid-span deflection (ratios) of four rectangular slabs were 67mm

(0.14mm/min), 66mm (2.5mm/min), 74mm (0.36mm/min) and 49mm (0mm/min), respectively. In addition, according to the deflection or deflection ratio failure criteria [23], i.e., the deflection or deflection ratio of the slab exceeds (l/30) l/20 or $l^2/(9000d)$ at any fire exposure time, and thus the fire resistance of each slab is shown in Table 4 based on a limiting deflection criterion.

Note that, during the heating stage the deflection curves of Slab R2 (R3) showed short deflection plateaus at 114 (99) and 144 (115) min, respectively. This behavior was not observed in square Slabs S1 to S4 [18] or rectangular Slab R4. It is suspected that the cause of such behavior is associated with displacement transducer hardware problems, since no deflection plateau occurred at other measurement points.

During the cooling stage, the vertical deflections of Slabs R1 to R4 are presented at 400min, 300min, 300min and 300min, respectively. On one hand, Figs. 8(a)-(d) show that the uniaxial (biaxial) restrained and unrestrained concrete slabs have different deflection recovery trends during this stage. For instance, Slab R1 had a nonlinear deflection recovery trend and its residual mid-span deflection was about 30mm (32) at 400 min (360), and the recovery value was about 56% (53%). However, the mid-span deflections of restrained Slabs R2 and R3 were recovered linearly during the cooling phase, but that of Slab R4 was recovered nonlinearly. The residual mid-span deflections of Slabs R2 to R4 were about 47 mm, 51mm and 35mm at 300 min, respectively and their recovery values were 29%, 32% and 29%, respectively. Clearly, the restrained slabs have lower recovery ratios, this is similar to that of Slabs S1 to S4 [18], indicating that the uniaxial or bi-axial in-plane forces are detrimental to the deflection recovery of the concrete slabs during the cooling phase. However, in the real building, the compressive restraint forces would normally change to tension at high deflection in order to resist pull-in of the edges. Hence, the concrete slabs with the various in-plane restraint should be further studies through the full-scale fire tests.

(2) Snap-through behavior and deflection reversal

As shown in Fig. 8(e), different from those of the other restrained slabs, Slab S5 had small hogging deflections before 60min, although the serious concrete spalling occurred during this stage. On one hand, as shown in Fig. 6(g), this is due to the temperature gradient (convex shape) through the thickness of Slab S5, which resulted in upward deflection. It is noted that the temperature gradient of other slabs was concave shape, as indicated in Fig. 6(h). According to the upward deflection, it can be concluded that the centroidal axis may be located lower than the applied force. In other words, the applied restraint forces produced a negative moment (arch effect), which reduced the positive moments at mid-span and increased the initial stiffness [12]. The reduction of the positive moments at mid-span allowed the slab to be exposed to fire for a longer time with small deflections. In addition, this increased stiffness also decreased the crack number or delayed the crack formation as discussed later. Thus, the comparison shows that the restrained slabs' deflection not only depends on the restraint force types and levels but also the temperature gradient.

However, as the tested continued, the material properties degraded, the centroidal axis of the slab changed, although the position of the applied forces was fixed at mid-depth of the slab. In other words, the position of line of the applied force might be located close to or above the centraoidal axis of the slab at the support, the applied compressive forces gradually became detrimental to the slab as they increased the moments, accelerated the deflections and led to the clear instability (snap through). As expected, after 60min, the vertical deflections increased suddenly. Note that, at 73min, the mid-span deflection (61mm) and ratio (15.6mm/min) of Slab S5 were not the maximum, but the maximum values at Point S5-V1 were 92mm and 24mm/min, respectively.

At the corresponding shut-off time, the deflection (82mm) and ratio (0.4mm/min) of Slab S6 and those of Slabs R1 to R4 were lower than those of Slab S5. On one hand, this is due to the serious concrete spalling within Slab S5, i.e., three holes were observed during the fire test. In addition, P-δ effect led to the rapid deflection of this restrained slab. During the initial stage, the in-plane force led to the accumulated high stresses within the restrained slab. With the decreased stiffness and material properties, the high stresses easily resulted in snap through or instability. However, different from the ambient tests of the restrained slabs [24], the rapid deflection and instability of the restrained slabs in fire were associated with the frequent and serious concrete spalling, which led to the deflection reversal (Fig. 8(e)). Hence, different from the ambient tests [24], the fire-resistant performance of the concrete slabs does not always increase with increasing axial restraint due to the interaction of the above behavior [25], especially the spalling.

During the cooling stage, different from the deflection recover of other slabs, the deflection of Slab S5 continued to rapidly increase, reaching 210mm and 153mm of Points S5-V1 and S5-V3 at 99min, respectively. Hence, it can be concluded that more serious failure occurred during the cooling phase, although the furnace temperature rapidly decreased with time. Additionally, the vertical deflection reversal of Slab S5 clearly appeared during the cooling phase, indicating the spalling occurred.

In all, according to the authors' knowledge, this deflection reversal behavior of the restrained slabs for the first time is clearly observed due to the interaction of the applied high restraint forces, serious spalling and the convex temperature gradient across the thickness.

2. Deflection-average furnace curves

Figs. 9(a)-(f) shows the vertical deflections versus average furnace temperature curves for Slabs R1 to R4, S5 and S6. On one hand, for Slabs R1 to R4 and S6, there are two deflection stages for each slab during the heating phase. When the furnace temperature was below 500°C or 600°C, the mid-span deflections of these slabs were relatively small. After that, the slabs rapidly deflected until the shut-off time. During the cooling stage, the vertical deflection-average furnace temperature curves of Slabs R1 to R4 and S6 show the similar development trends and can also be divided into two stages. Note that this conclusion is similar to that of Slabs S1 to S4 [18] and other slabs' tests [28-29]. Hence, it can be seen that the furnace temperature has a considerable effect on the fire behavior of the concrete slabs with different boundary conditions.

However, as expected, the deflection-average furnace curves of Slab S5 were different from those of other restrained slabs during the heating and cooling stages. For instance, the average furnace temperature reached about 730°C, the deflections began to sharply increase. Clearly, during the heating stage, the temperature was postponed due to the high in-plane bi-axial restraint. During the cooling stage, the deflection rapidly increased after about 300°C and then fluctuated due to concrete spalling.

3.2.2 Horizontal deflections

Fig. 10 shows the measured horizontal deflections (Point H1) of six concrete slabs, and there are different horizontal deflection trends among these slabs due to the effect of the uniaxial or biaxial in-plane restraint forces.

As shown in Fig. 10, Slab R1 expanded at a linear ratio until 100 min and followed by a plateau between 100 and 240 min. The plateau may be due to the interaction between the expansion (increasing temperature) and the contraction (downward deflection). The deflection trend of the rectangular slab R1 is similar to the observation in [3]. In addition, for Slab R2, it expanded at a liner rate until 180 min and reached 23.3mm. As expected, due to the effect of the uniaxial in-plane force [18], the horizontal deflection of Slab R2 was always larger than that of Slab R1 during the heating stage. Meanwhile, the horizontal deflection trends of the Slabs R3, R4 and S6 were similar to that of Slab R1, particularly the plateau at the later stage. However, it is evident that the mechanical mechanism (bi-axial restraint) for the plateau of Slabs R3, R4 and S5 was different from that of Slab R1.

Different from other restrained slabs, the horizontal deflection of Slab S5 was positive (contraction) until 60min due to the high in-plane restraint forces. After that, Slab S5 suddenly expanded up to 42mm and followed with recovery behavior, this may be due to the snap through as discussed above. However, it is suspect that the slab's translational motion occurred at that time. At 73min, its horizontal deflection was the maximum and was

32mm.

During the cooling stage, Slabs R1 and R2 immediately contracted nonlinearly, and their residual horizontal deflections were 1.5mm and 15.3mm at the end of each test, respectively. However, due to the bi-axial restraint, Slabs R3 and R4 slightly contracted during the initial cooling stage, reaching a plateau, and then were followed by a slower linear contraction trend until the end of the test, with the residual horizontal deflections of 0.5 mm and 14.1 mm, respectively. In addition, for Slab R5, similar to its out-of-plane deflections, its horizontal deflection significantly fluctuated with time because of serious spalling. For Slab S6, its horizontal deflection basically kept constant (5.5mm) until the end of the fire test due to the bi-axial restraint.

In all, the in-plane restraint forces and types have an important effect on the horizontal deflection trends during heating and cooling stage. Specifically, the uniaxial restraint forces lead to the larger horizontal deflections and higher deflection recovery ratios perpendicular to the restraint forces direction, but the bi-axial in-plane restraint forces tend to result in the smaller horizontal deflections and lower recovery deflection.

3.3 Restraint forces

In the following section, restrained forces for six slabs are briefly discussed in the paper, including the in-plane compressive force applied by each jack and the reaction forces at the corners of each slab. It is noted that the positive forces indicate the compressive forces during the tests.

3.3.1 In-plane forces

(1) Slab R2

As discussed above, Slab R2 was tested under the uniaxial in-plane (N-S direction) and out-of-plane loads. During the test, the applied uniaxial in-plane stress was 2 MPa, and thus the force applied by each jack should be 220 kN. Fig. 11 shows the uniaxial in-plane forces measured from the pressure sensors P-5 to P-7 with their average values.

As the test started, the applied forces at Points P-5 to P-7 increased rapidly from 202kN, 208kN and 199kN due to the expansion, reaching the maximum values of 229kN (62min), 228kN (63min) and 244kN (90min), respectively, with the increasing rate of 13.4%, 9.6% and 22.6%, respectively. After that, the in-plane forces at three points showed different development trends, but their average values gradually decreased until 180min. During the cooling stage, the average in-plane forces rapidly increased up to 227kN (at 220min), and then gradually decreased until the end of the fire test.

Clearly, due to the complexity of fire test, it was very difficult to keep the applied in-plane forces constant

(220kN). However, according to the average curves, the in-plane force during the fire test was about 221kN, and thus it basically satisfied the test requirement of 2MPa.

(2) Slab R3

Slab R3 was tested under different biaxial in-plane forces in the two directions. In other words, the in-plane stresses were 2MPa (N-S direction) and 1MPa (W-E direction), respectively. Figs. 12(a) and 12(b) show the in-plane forces measured from the pressure sensors P-5 to P-7 and P-8 to P-10 with the corresponding average values, respectively.

As shown in Fig. 12(a), as the fire started, the applied forces at Points P-5 to P-7 kept constant (234kN, 219kN, and 227kN) until 60min, with the average value of 227kN. After that, the forces at Points P-5 and P-7 gradually increased and reached at a plateau between 120 and 190min, with the maximum values (increasing ratio) of 258kN (10.3%) and 270kN (18.9%), respectively. In addition, at Point P-6, the force increased between 60 and 120 min, reaching about 256kN (14.2%) at 120 min, and then gradually decreased until 190min. During the cooling stage, the in-plane forces at three points showed different trends, but their average values basically remained constant. In all, according to the average values, the in-plane force applied by each jack was 242kN (2.2MPa) during the entire fire test.

As shown in Fig. 12(b), only two jacks were used to apply the in-plane restraint forces in the W-E direction, because the jack at Point P-9 malfunctioned in the fire test. Clearly, during the entire fire test, the in-plane forces can be considered to be constant. In addition, the maximum increasing ratios at Points P-8 and P-10 were 9.2% and 9.6% during the heating stage, respectively. Similarly, according to the average curve, the in-plane force applied by each jack was 203kN, with the stress of about 1.0MPa.

Hence, in the simply numerical or theoretical analysis, for Slab R3, the stresses applied in the N-S and W-E directions can be considered to be 2.2MPa and 1.0MPa, respectively.

(3) Slab R4

Slab R4 was tested under the same biaxial in-plane forces in the two directions during the fire test, as shown in Table 1. Fig. 13(a) shows the in-plane forces (N-S direction) measured from the pressure sensors P-5 to P-7, with the average curves. Clearly, unlike the previous two tests, the data fluctuated at the early stage, indicating that the internal force redistribution drastically occurred in the slab. After that, the in-plane forces at Points P-6 and P-7 slightly fluctuated and gradually decreased until the end of the fire test. In addition, the forces at Point P-6 (P-7) ranged from 184kN (167kN) to 238kN (246kN). However, at Point P-5, some “jump” behaviour of in-plane forces can be seen and it ranged from 176kN to 238kN, and then basically kept constant. Thus, compared to the uniaxial restrained slabs, the internal force redistribution was more serious in Slab R4 during the entire test. Similarly, the average curves indicate that the N-S in-plane forces was constant during the test, with the average value (stress) of 220kN (2.0MPa).

Fig.13 (b) shows the in-plane forces at Points P-8 to P-10 in the test. Clearly, the in-plane forces at three points rapidly increased during the early stage, and then considerably fluctuated in W-E direction. In other words, the big “jump” behaviour was observed between 5min and 40min due to the drastic internal force redistribution, and then followed by different development trends. For instance, the forces at Point P-8 (9, 10) ranged from 86kN (133kN, 57kN) to 232kN (292kN, 264kN). After that, the in-plane forces at three points gradually kept constant until the end of the fire test. In addition, it is noted that the average value of restraint forces basically remained constant during the whole fire test, with the stress of 1.6MPa.

(4) Slabs S5 and S6

Slab S5 was tested under the biaxial in-plane forces in the two directions during the fire test, as shown in Figs. 14(a) and 14(b). As shown in Fig. 14(a), there were large differences among the three in-plane forces, particularly at Point P-7 (hardware problem). In other words, the in-plane restraint forces at Points P-5, P-6 and P-7 gradually increased from 280kN, 309kN and 89kN until about 70min, followed by the sudden “jump” due to the snap through. The maximum increasing ratios at three points were 7.1%, 11% and 37.1%, respectively. After that, the in-plane forces gradually decreased until the end of the fire test. However, it is interesting to note that the average curves during the fire test basically kept constant, with the average value (stress) of 227kN (2.1MPa). As shown in Fig. 14(b), compared to the in-plane forces in the N-S direction, the smaller difference appeared among the three in-plane forces at Points P-8 to P-10. Similar to those observed in Fig. 14(a), there were some small “jump” of each force at about 70min. In addition, the maximum increasing ratio at Point P-8 was 28.1%. In all, according to the average curves, the in-plane force applied by each jack was about 213kN, with the stress of 1.95MPa.

Slab S6 was tested under different biaxial in-plane forces in the two directions during the fire test, as shown in Figs. 15(a) and 15(b). Similar to those of Slab S5, the in-plane forces at Points P-5, P-6 and P-7 firstly increased from 243kN, 237kN and 242kN with time, and suddenly decreased until the end of the fire test. The maximum increasing ratios were 32.1%, 5.5% and 21.5%, respectively. For the W-E direction, the applied restraint force at Points P-8 and P-10 gradually increased and reached a plateau, and that at Point P-9 kept constant during the fire test. In addition, the maximum increasing ratio at Point P-10 was 39.8%. Hence, the average in-plane forces (stress) in the two directions were 251kN (2.28MPa) and 136kN (1.24MPa), respectively.

In all, the average in-plane forces in each direction have similar development trends during the heating and cooling stages. Specifically, they firstly increased due to the expansion, and then gradually decreased or kept constant until the end of the fire test. No doubt, to some degree, the present results imply the in-plane restraint development trends of the floor in the actual buildings.

3.3.2 Corners forces

The variations of the restrained forces at the four corners of each slab were measured during the fire tests. The main observed results are briefly presented in the following sections.

(1) Slabs R1 and R2

Fig.16 (a) shows the reaction forces measured by the pressure sensors (Points P-1 to P-4) at four corners of the slab. It is apparent that the reaction forces started from 0kN and showed similar trends during the fire test. During the initial stage, the force at each corner rapidly increased. After 20min, the reaction forces at the four corners showed a little different trends due to the diagonal cracks. It is interesting to note that the reaction forces at four points basically kept constant between 100 and 240min. During the cooling stage, the reaction forces at Points P-1, P-3 and P-4 gradually decreased, and reached 0kN at about 260min. In addition, the data at Point P-2 were not recorded at 230min due to the hardware problem.

Fig. 16(b) shows the reaction forces measured by pressure sensors (Points P-1 to P-4) during the fire test. Similar to those of Slab R1, the reaction forces at four corners rapidly increased and reached the maximum values before 70min. For instance, Points P-1 to P-4 reached the maximum values (8.9kN, 9kN, 2.9kN, and 6.8kN) at 48min, 40min, 61min and 63min, respectively. Clearly, due to the in-plane restraint, the maximum reaction forces of Slab R2 were larger than those of Slab R1. This conclusion is similar to the observation in Slabs S1 to S4 [18]. After 70min, as expected, the corners' reaction forces showed different trends. For instance, the force at 44min sharply decreased from 9kN to 0.5kN, because the crack at Point P-2 suddenly appeared. In contrast, the three corners still had better load-carrying capacities until the end of the fire test.

(3) Slabs R3 and R4

Figs. 16(c) and 16(d) show the restraint forces at four corners of Slabs R3 and R4 during the fire test. Note that, in Slab R3, the data at Point P-1 were not recorded due to the hardware problems. Clearly, there are different development trends among the corners' forces in the two rectangular slabs.

For Slab R3, the reaction forces at Points P-2, P-3 and P-4 were 10.6kN, 4.0kN and 2.7kN, respectively, and then kept constant until 60min. After 60min, the reaction forces at Points P-2 and P-3 gradually decreased, followed by the increase, and reached 9.9kN and 6.3kN at 300min, respectively. However, at Point P-4, the reaction forces gradually increased until 95min, and then rapidly decreased to 0kN at 164min. Similarly, the maximum restraint forces within Slab R3 was higher than those of Slab R1 due to the bi-axial in-plane forces.

For Slab R4, as the test started, the reaction forces at four corners rapidly increased, followed the different trends until the end of the fire test. Clearly, the maximum restraint forces of Slab R4 were higher than those of Slab R3, due to less corners' cracks, as discussed later. For instance, the reaction forces at Points P-1 to P-4 reached the maximum values of 16kN (90min), 7.4kN (77min) 16kN (39min) and 7kN (55min), respectively. And then, the corners' failure at Points P-2 and P-3 suddenly occurred, but the reaction forces at Point P-1 kept higher values until the end of the fire test. Hence, although the bi-axial in-plane restrained forces are beneficial to enhance the corners' carrying capacities, the corners' brittle failure easily occurs during the heating stage.

(5) Slabs S5 and S6

The reaction forces at each corner of Slabs S5 and S6 are plotted against time, as shown in Figs. 16(e) and 16(f). Note that the force at Point P-2 was not recorded due to the hardware problem, but the corner was clamped in each test.

On one hand, during the initial stage, there are similar trends among three reaction forces within Slab S5. However, the reaction forces existed larger difference, and the maximum restraint forces at three points were 2.7kN, 7.4kN and 10.3kN, respectively. On the other hand, for Slab S6, the reaction forces rapidly increased and then decreased until the end of the fire test. Note that, due to the higher stiffness, the maximum restraint forces at Points P-1, P-3 and P-4 of Slab S6 were 14.4kN, 14.0kN and 8.9kN, respectively, which were larger than those of Slab S5.

In all, according to the present results, it can be concluded that the in-plane compressive forces applied in the slabs have an important effect on the initial values, development trends and maximum values of the corners' restraint forces during the fire test. In addition, compared to the simply supported slabs, the uniaxial or bi-aixal in-plane restrained slabs have the higher carrying capacities at their corners. However, due to no top steels within six slabs, their corners easily fractured during the heating stage. Note that, the corners' failure may easily lead to the shear failure of the slab at large deflections before its tensile membrane action sufficiently develops. Hence, the experimental results further indicate that the top steels should be placed within the slabs, since they are beneficial to enhance the fire resistance of the slabs' corners and develop the tensile membrane action.

3.4. Structural failures

3.4.1 Observations

During the heating stage, the six concrete slabs were inspected for the test phenomena and an explanation is provided for the observed behaviors. After test, visual signs of cracking and spalling were investigated and photographic evidence of the failure modes is presented in this paper.

(1) Slab R1

Fig. 17(a) shows the top view of Slab R1 after the fire. Cracks were darkened with a brush to make them visible in the photograph. Clearly, two visible cracks on the top surface of the slab was forming across the shorter span of the rectangular slab. In addition, there were several large cracks near to the four corners. These cracking patterns are similar to those observed in the [3].

During the early stage of the fire, several pop-ping noises were firstly heard from the slab's bottom surface between 15min and 20min. At 20 min, a crack ① formed at the south-east corner of the slab, as shown in Fig. 17(b). Meanwhile, water steam was emitted from the crack as the test continued. At 33min, one loud sound (spalling) was heard from the bottom surface of the slab. At 42min, one crack ② was parallel to the west-east direction and at 1/2 span from the edge. Between 43min and 56min, several loud sounds (spalling) were heard and one small crack ③ normal to the edge occurred, which was at approximately 1/2 span. Meanwhile, a large amount of water and steam also seeped through the cracks, forming a puddle of water owing to the water accumulation. Between 83 min and 100min, the diagonal cracks ④, ⑤ and ⑥ on the top surface successively occurred, leading to the decreased restraint forces (Fig.16(a)). These cracks resulted from the holding down of the slab corners. As the test progressed, the cracks on top surface of the slab continued to widen, particularly the diagonal cracks at the corners. For instance, at 150min, the width of the crack ② was about 5mm.

Figs. 17(c) and 17(d) show the bottom view of the slab after the fire. Serious concrete spalling occurred, and thus reinforcing bars can be seen on the bottom surface of the slab. It is noted that the spalling area and maximum depth were about $2.64m^2$ and 70mm, respectively. In addition, as shown in Fig.17(c), two cracks across the short span appeared on the bottom surface, which were corresponding to the top surface cracks ① and ② (Fig.17(b)), indicating the integrity failure occurred. Meanwhile, some diagonal cracks running at 45^o from the corners towards the central region and some cracks normal to the edges could also be seen on the bottom surface. This observation is similar to the tested rectangular slabs reported in [3].

Note that, the cracking pattern of rectangular Slab R1 is compared with that of square Slab S1 [18]. The obvious difference is that no crack across any whole span appeared on the top and bottom surfaces of Slab S1 [18], indicating that the aspect ratio has an important effect on the cracking pattern of the simply supported slabs.

(2) Slabs R2

Figs.18 (a) and 18(b) show the cracking pattern on the top surface of Slab R2 under the uniaxial restrained forces. At 14min, the crack ① normal to the edge first appeared on the top surface of the slab, as shown in Fig.18(b). Clearly, this is consistent with that of Slab R1. At 20min, the sound (spalling) was heard, and the crack ① width increased with time. Between 20 and 40min, water and steam seeped through the crack. At 40min, the crack ② appeared on the north-east corner of the slab. At 45min, the north-east corner suddenly fractured with the crack ② width of 5mm, which led to the sudden decrease of the restraint forces at Point P-2 (Fig. 16(b)). After that, the cracks ③ and ④ appeared on the north-west and south-west corners of the slab, respectively, which also led to sudden and gradual decrease trends of restraint forces at Points P-1 and P-4 (Fig. 16(b)). This indicates that the corners' cracks position has an important effect on the restraint forces of the slabs. In addition, it is noted that the spalling (sound) occurred between 40 and 60min.

Clearly, the cracking pattern of Slab R2 was different from that of Slabs R1 and S1 [18], but similar to that of uniaxial restrained Slabs S2 to S4 [18]. Hence, the in-plane forces have an important effect on the failure mode of the concrete slabs in fire and its effect should be reasonably considered in the theoretical analysis.

Figs.18(c) and 18(d) show the spalling and cracking pattern on the bottom surface of Slab R2. It can be seen that the concrete cover had fallen off and reinforcement bars could be seen. Clearly, the area of spalling ($0.45m^2$) was smaller than that of Slab R1 due to the effect of the in-plane restraint forces, but the maximum depth (90mm) of spalling was larger than that of Slab R1. In addition, one crack formed across the long span, and this observation is similar to that of Slab S2 under uniaxial restraint [18]. The whole length crack is easily formed in the slab under the uniaxial in-plane forces due to the Poisson's effect, as discussed in [18]. Meanwhile, the diagonal cracks occurred near to each corner, and the fracture of north-east and north-west corners and concrete crushing can be seen on the bottom surface. Hence, the failure mode of Slab R2 was the material failure (concrete crushing and corners' fracture) associated with the integrity failure (whole length crack).

(3) Slabs R3, R4, S5 and S6

Figs. 19(a)-22(d) show the failure models of the bi-axial restrained Slabs R3, R4, S5 and S6, but the cracks' development and the sound (spalling) during the heating stage are not discussed in detail.

On one hand, for the rectangular Slabs R3 and R4, their cracking patterns are similar to each other, but different from that of the square Slabs S5 and S6. For instance, for Slabs R3 and R4, one or two cracks across the long and short spans appeared on the top surface with many longer cracks. In contrast, for Slabs S5 and S6, apart from the corners' cracks, one whole span crack parallel to the larger in-plane forces can be seen on the top surface. Meanwhile, three holes appeared in Slab S5 due to the serious spalling. It is found that the crack patterns of Slabs S5 and S6 were similar to those of Slabs S2 to S4 under uniaxial restraint, but different from that of the simply supported Slab S1 [18].

On the other hand, little concrete spalling, fewer cracks and no whole length crack were observed on the bottom surfaces of Slabs R3 and R4, regardless of the higher biaxial in-plane forces. In contrast, as shown in Figs. 21(c) and 22(c), very serious spalling occurred on the bottom surface of Slabs S5 and S6 with the fewer corners' cracks, particularly Slab S5. For instance, the spalling areas of Slabs S5 and S6 were 5.3m^2 and 0.7m^2, respectively, with the maximum depth of 100mm (holes) and 45mm.

The comparison indicates that Slabs R3 and R4 occurred with the material failure due to the concrete crushing at the corners. However, Slab S5 occurred with the material failure (serious spalling), integrity failure (holes) and the instability (snap through and deflection reversal), Slab S6 reached the material failure (serious spalling and corners' fracture). Hence, the slenderness ratio, the restraint types and levels have an important effect on the restrained slabs' failure modes, and the restrained slabs often had several failure modes.

In addition, as discussed in [18], the uniaxial restrained slabs (Slabs S2 to S4) easily occurred with the integrity failure due to the full depth cracks. In contrast, without consideration of the spalling, the bi-axial restraint forces may be beneficial to prevent the whole span full-depth cracks (integrity failure) within the restraint rectangular and square slabs, as indicated in Figs. 19(c), 20(c) and 22(c). In fact, the experimental results is similar to those observed in the recent fire tests of the floor in the steel-framed building [5-7]. For instance, as reported in [6], fewer cracks and no spalling appeared on the bottom surface of the floor, even though the heating lasted about 5 hour. This is due to the fact that the bi-axial restraint may prevent the Poisson's effect.

3.4.2 Failure criteria

The conventional method of evaluating the slabs' fire resistance is based on the thermal and deflection failure criteria [26], as shown in Section 3 and Table 4. Clearly, because the effect of the boundary conditions is not considered in the four failure criteria, the slabs' fire resistances are overestimated and not conservative, particularly the deflection failure criteria.

In fact, in recent years, several new theoretical methods were developed based on different failure criteria and failure modes. For instance, Bailey [1-2] proposed one theoretical method to determine the fire resistance of the concrete slabs, and three assumptions are: the yield line failure mode, no in-plane restraint and the deflection failure criterion. Similarly, based on yield line failure mode and steel strength failure criterion, two theoretical models (CM and IM models) were proposed by Omer et. al [30-31] to determine the load-carrying capacities of the unrestrained slabs in fire. Meanwhile, Cashell et.al [32] further developed Omer's analytical model by considering the concrete crushing within the unrestrained slabs. In addition, different from Bailey's model [1-2] and Omer's model [30-31], Cameron and Usmani [33] proposed one energy method for calculating the tensile membrane capacity of laterally restrained slabs (free to rotate) in fire with the steel strain failure criterion. In 2007, based on equilibrium of the forces and bending moments (four rigid plates and an elliptic paraboloid), Li et al. [16-17] proposed the steel strain failure criterion to determine the load-carrying capacities of the in-plane restrained slabs. Clearly, the single steel failure criterion was often used in the theoretical methods. However, as discussed above, several failure modes of the present restrained slabs occurred, including the integrity failure (Slab R1), the serious spalling (Slabs R1, R2 and S5), corner's fracture (Slabs R1, R2, R3, R4 and S6) and the instability (Slab S5). Hence, it can be conclude that the single factor failure criterion may be not reasonable, and should be modified by considering the detrimental effect of the in-plane restraint on the load-carrying capacities of the slabs.

In all, the failure modes of the concrete slabs in fire, however, are relatively complex because of the large number of interrelated variables that influence the response, particularly the in-plane restraint. On one hand, different in-plane restraint types and levels lead to different cracking pattern of the restrained slabs. More importantly, before reaching the load carrying capacities or steel failure, two or three failure modes often appear within the restrained slabs, including the integrity failure, corners' fracture or serious concrete spalling. Hence, prediction of the fire behavior corresponding to failure necessitates a detailed treatment of the interaction between the material properties and the boundary conditions [32].

3.4.3 Discussion

Based on the observations of six concrete two-way slabs in fire, following conclusions can be drawn:

(1) For the in-plane unrestrained or restrained slabs, diagonal cracks (45^{o}) can be seen near to the slab's

corners due to the twisting action (clamped corners). Meanwhile, the corners' fracture often occurs during the early stage of the heating, which may result in possible shear failure of the slabs at large deflection. Hence, the fire-resistant design should be used to enhance the load carrying capacities of the slab's corners.

(2) For any slabs, at the initial stage, the reaction forces at the four corners have the similar development trends (decrease, increase or constant) with different values. With the increasing temperatures, there are different trends due to the various crack numbers, position or the sudden fracture. In addition, compared to those of the simply-supported slabs or the un-axial restrained slabs, the bi-axial in-plane restraint leads to the higher corners' restraint forces during the fire test.

(3) For the uniaxial in-plane restrained slabs (Slabs S2 to S4 [18] and R2), one or two whole length cracks parallel to the restraint force often appeared on the top surfaces. Clearly, these whole length cracks were due to the Poisson's effect, different from the flexural cracks observed in Slabs S1 [18] and R1. Hence, the failure modes of the uniaxial in-plane restrained slabs are different from those of two simply-supported slabs.

(4) For the bi-axial restrained slabs (Slabs R3, R4, S5 and S6), the in-plane forces and slenderness ratio have an important effect on their failure modes. The material failure (corns' fracture or concrete crushing) and instability was reached for the slabs with the bi-axial restraint. More importantly, the obvious snap through and deflection reversal for the first time were observed in Slab S5 due to its abnormal temperature gradient across the thickness (convex shape) and serious spalling. Hence, compared with other failure modes, the instability with spalling is very detrimental to the development of tensile membrane action and should be prevented through the reasonable fire-resistant design.

(5) The conventional yield-line failure mode and failure criteria for the simply supported slabs may not be appropriate for predicting the fire resistance of the uniaxial or biaxial restrained slabs.

(6) How to model the cracks and concrete spalling is the key problem to accurately understand the mechanical mechanism (snap through or deflection reversal), localised concrete failure (corner fracture or full-depth cracks), and bottom surface's spalling of the restrained slabs in fire. Hence, according to the experimental results, numerical work will be conducted to understand the fire behavior of the restrained slabs.

4. Conclusions

Six full-scale fire tests on reinforced concrete slabs, under combined in-plane and out-of-plane loading conditions with vertical restraint at four corners of the slabs, are presented in this paper. Based on the experimental observations, following conclusions are drawn:

(1) During the heating and cooling stages, vertical and horizontal deflection trends of the slabs with uniaxial or bi-axial in-plane restraint are significantly different from those of the simply supported slabs. In addition, compared to the simply supported slab, the restrained slabs tend to have larger vertical and horizontal deflections at the later stage of the fire tests with the lower deflection recovery during the cooling stage.

(2) Cracking patterns of the restrained slabs depend mainly on the uniaxial or biaxial in-plane levels. For any in-plane restrained slabs, one or two cracks across one or two whole spans certainly appear on the top surface of the slabs as well as diagonal cracks near to the corners. However, number, direction and position of cracks for the bi-axial restrained slabs are considerably different from those of the slabs with or without the uniaxial restraint forces.

(3) The uniaxial or biaxial in-plane force levels have a significant effect on the failure behavior of the restrained slabs, including cracking patterns, concrete spalling, corners' fracture, instability (snap through) and integrity failure. Hence, the conventional yield-line failure mode and failure criteria are not suitable for the in-plane restrained slabs, and the effect of uniaxial or bi-axial in-plane restraint forces should be reasonably considered to establish their corresponding failure modes and failure criteria.

The experimental results and comparisons discussed here can be used to develop the numerical or theoretical models. Such models will further clarify the observed behavior and provide knowledge and insight for answering numerous questions or theoretical questions regarding fire-resistant performance of restrained slabs.

Acknowledgements

This research was supported by the National Natural Science Foundation of China (Grant No. 51408594) and Fundamental Research Funds for the Central Universities (Grant No.2014QNA78). The authors gratefully acknowledge this support.

References

[1] Bailey C.G, Toh W.S., Behaviour of concrete floor slabs at ambient and elevated temperatures, Fire Safety Journal, 2007, 42: 425-436.

[2] Bailey C.G., Toh W.S., Small-scale concrete slab tests at ambient and elevated temperatures, Engineering

Structures, 2007, 29: 2775-2791.

[3] Lim L., Wade C., Experimental fire tests of two-way concrete slabs, Fire Engineering Research Report 02/12, University of Canterbury and BRANZ Ltd, New Zealand, 2002.

[4] Dong Y.L., Zhu C.J., Limit load carrying capacity of two-way slabs with two edges clamped and two edges simply supported in fire, Journal of Structural Engineering, 2010, 137: 1182-1192.

[5] Yang Z.N., Dong Y.L., Xu W.J., Fire tests on two-way concrete slabs in a full-scale multi-storey steel-framed building, Fire Safety Journal, 2013, 58: 38-48.

[6] Wang Y., Dong Y.L., Li B., Zhou G.C., A fire test on continuous reinforced concrete slabs in a full-scale multi-story steel-framed building, Fire Safety Journal, 2013, 61: 232-242.

[7] Li B., Dong Y., Lou Y.J., A fire test of continuous panels in a full-scale steel-framed structure, Engineering Mechanics, 2015, 32: 145-153. (in Chinese).

[8] Selvaggio S. L., Carlson C. C., Effect of restraint on fire resistance of prestressed concrete. American Society for Testing and Materials, STP 344, 1963, 1-25.

[9] Issen, L. A, Gustaferro, A. H, and Carlson, C. C. Fire tests of concrete members: An improved method for estimating thermal restraint forces. Fire Test Performance, ASTM, 1970, 153-185.

[10] Lin T.D., Zwiers R.I., Shirley S.T., Burg R.G., Fire test of concrete slab reinforced with epoxy-coated bars, ACI Structural Journal, 1989, 86:156-162.

[11] Cooke G.M.E., Results of tests on end-restrained reinforced concrete floor strips exposed to standard fires, Report Prepared for the Construction Directorate of the Department of the Environment, Fire Research Station, Hertfordshire UK, 1993.

[12] Lim L., Buchanan A., Moss P., Franssen J.M., Computer modeling of restrained reinforced concrete slabs in fire conditions, Journal of Structural Engineering, 2004, 130: 1964-1971.

[13] Huang Z., Burgess I.W., Plank R.J., Modeling membrane action of concrete slabs in composite buildings in fire. I: Theoretical development, Journal of Structural Engineering, 2003, 129: 1093-1102.

[14] Huang Z., Burgess I.W., Plank R.J., Modeling membrane action of concrete slabs in composite buildings in fire. II: Validations, Journal of Structural Engineering, 2003, 129: 1103-1112.

[15] Cameron N.J.K, Usmani A.S., New design method to deterimine the membrane capcity of laterally restrained composite floor slabs in fire Part 1: Theory and method, The Structural Engineer, 2005, 83(19): 28-33.

[16] Li G.Q., Guo S.X., Zhou H.S., Modeling of membrane action in floor slabs subjected to fire, Engineering Structures, 2007, 29: 880-887.

[17] Zhang N.S., Li G. Q., An innovative analytical method for the membrane action of composite floor slabs in fire, China Civil Engineering Journal, 2009, 42(3): 29-35.(in Chinese)

[18] Wang Y., Yuan G.L, Huang Z.H, et.al, Experimental study on the fire behavior of reinforced concrete slabs under combined in-plane and out-of-plane loads. Engineering Structures, 2016, 128: 316-332.

[19] Lim L., Buchanan A., Moss P., Franssen J.M., Numerical modelling of two-way reinforced concrete slabs in fire, Engineering Structures, 2004, 26: 1081-1091.

[20] Standard Methods for Testing of Concrete Structures of China (GB50152-92), (1992), Beijing. (in Chinese).

[21] Load code for the design of building structures (GB50009-2001), (2006), Beijing. (in Chinese).

[22] ASTM Standard methods of fire test of building construction and materials. Test Method. West Conshohocken, PA: American Society for Testing and Materials; 2001. p. E119-E201.

[23] BS. Fire tests on building materials and structures-Part 20: Method from determination of the fire resistance of elements of construction (general principles), BS476-3:1987, BSI, UK, 1987.

[24] Ghoneim M.G, McGregor J.G, Tests of reinforced concrete plates under combined inplane and lateral loads, ACI Struct J, 1994, 91:19-30.

[25] Dwaikat M.B., Kodur V.K.R., Hydrothermal model for predicting fire-induced spalling in concrete structural systems, Fire Safety Journal, 2009, 44: 425-434.

[26] Kodur V.K.R., Dwaikat M., A numerical model for predicting the fire resistance of reinforced concrete beams, Cement & Concrete Composites, 2008, 30:431-443.

[27] Banerjee D. K., An analytical approach for estimating uncertainty in meausred temperatures of concrete slab during fire, Fire Safety Journal, 2016, 82:30-36.

[28] Wang B, Dong Y.L, Experimental research of four-edge simple support two-way reinforced concrete slab under fire [J], Journal of Building Structures, 2009, 30(6): 23-33. (in Chinese)

[29] Wang B, Dong Y.L, Experimental research of two-way reinforced concrete slabs under fire, China Civil Engieering Journal, 2010, 43(4): 53-62. (in Chinese)

[30] Omer E., Izzuddin B.A., Elghazouli A.Y.. Failure of unrestrained lightly reinforced concrete slabs under fire, Part I: Analytical models, Engineering Structures, 2010, 32: 2631-2646.

[31] Omer E., Izzuddin B.A., Elghazouli A.Y.. Failure of unrestrained lightly reinforced concrete slabs under

fire, Part II: Verification and application, Engineering Structures, 2010, 32: 2647-2657.

[32] Cashell K.A., Elghazouli A.Y., Izzuddin B.A., Failure assessment of lightly reinforced floor slabs II: Analytical studies, Journal of Structural Engineering, 137(9): 989-1001.

[33] Cameron N.J.K., Usmani A.S.. New design method to determine the membrane capacity of laterally restrained composite floor slabs in fire Part 1: Theory and method, The Structrual Engineer, 2005, 83(19): 1-6.

[34] Huang Z. H., The behaviour of reinforced concrete slabs in fire, Fire Safety Journal, 2010, 45:271-282.

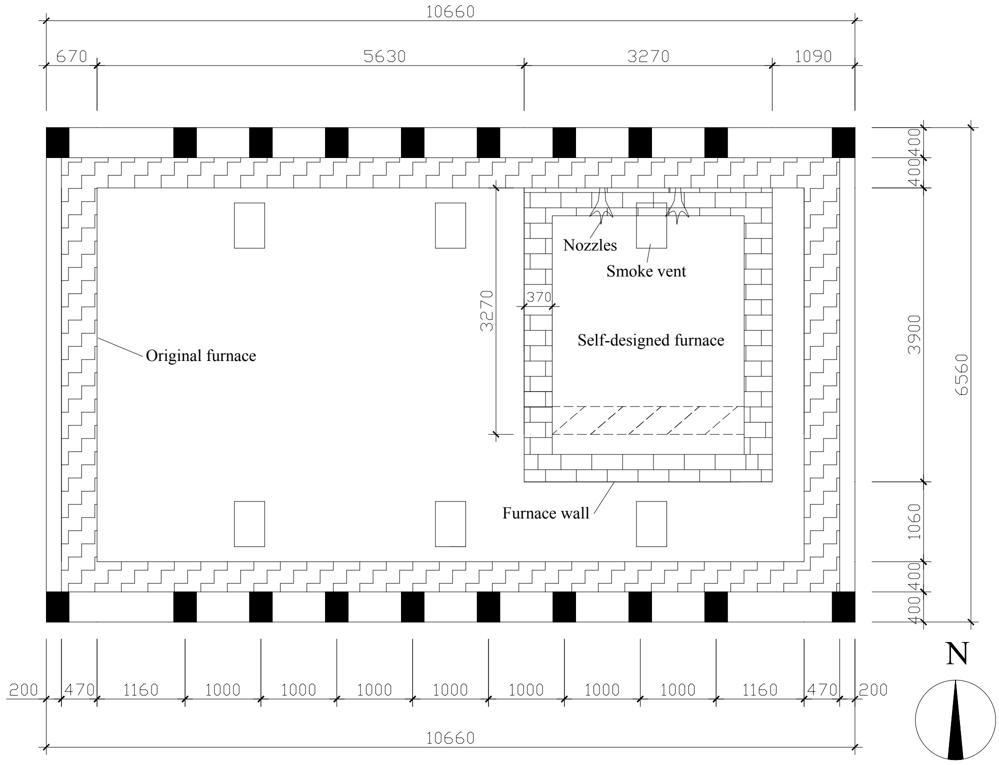

(a) Plan view of the furnace

(b) External view of the self-designed furnace

Fig. 1. Self-design furnace (all dimensions in mm).

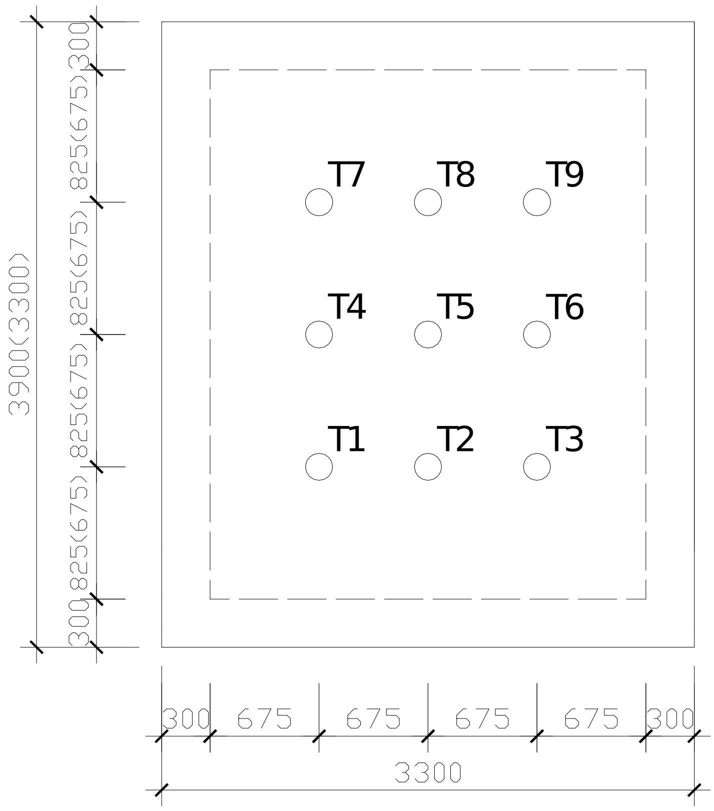

(a) Typical layout of thermocouples in the concrete rectangular (square) slab

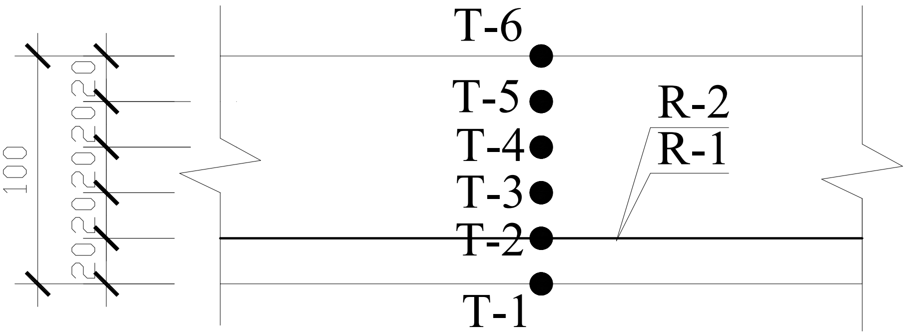

(b) Thermocouples across the full-depth of each slab

Fig. 2. The details of thermocouples' distribution within the slab
(all dimensions in mm)

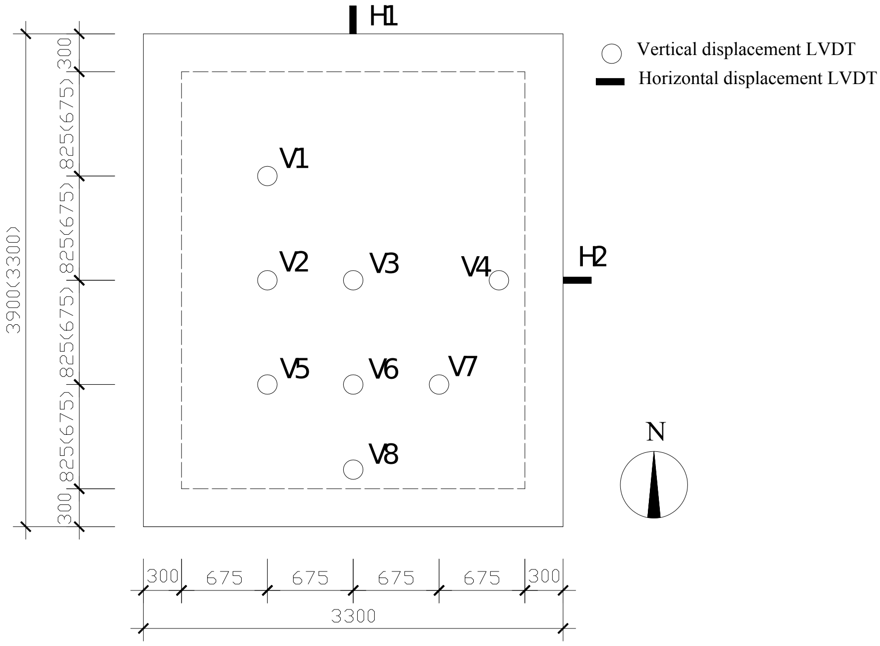

Fig. 3. Layout of the vertical and horizontal displacement transducers in rectangular (square) slab (all dimensions in mm).

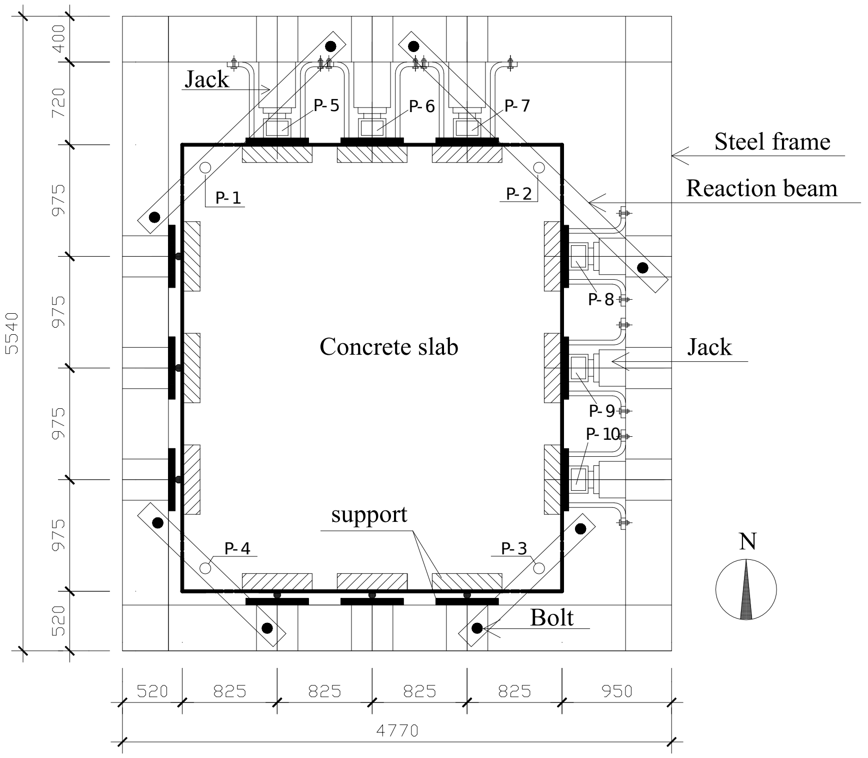

(a) Plan view of bi-axial in-plane loading frame

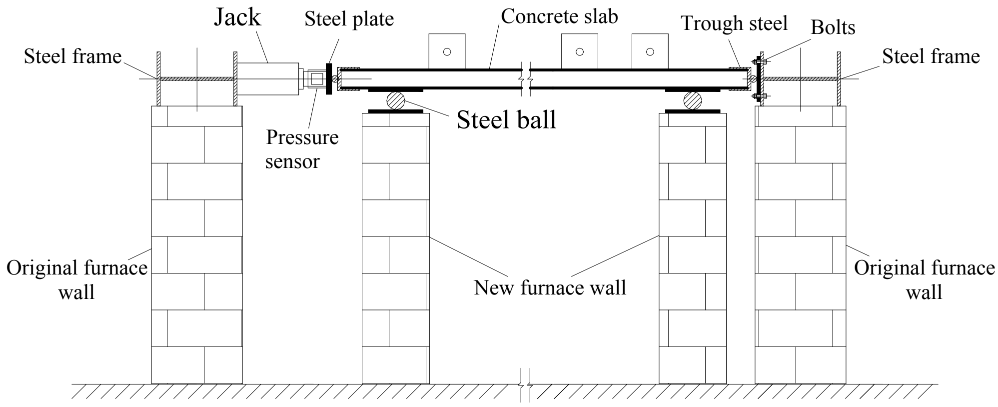

(b) Cross-section view of in-plane loading frame

Fig. 4. The details of horizontal bi-axial in-plane loading and vertical support systems (all dimensions in mm).

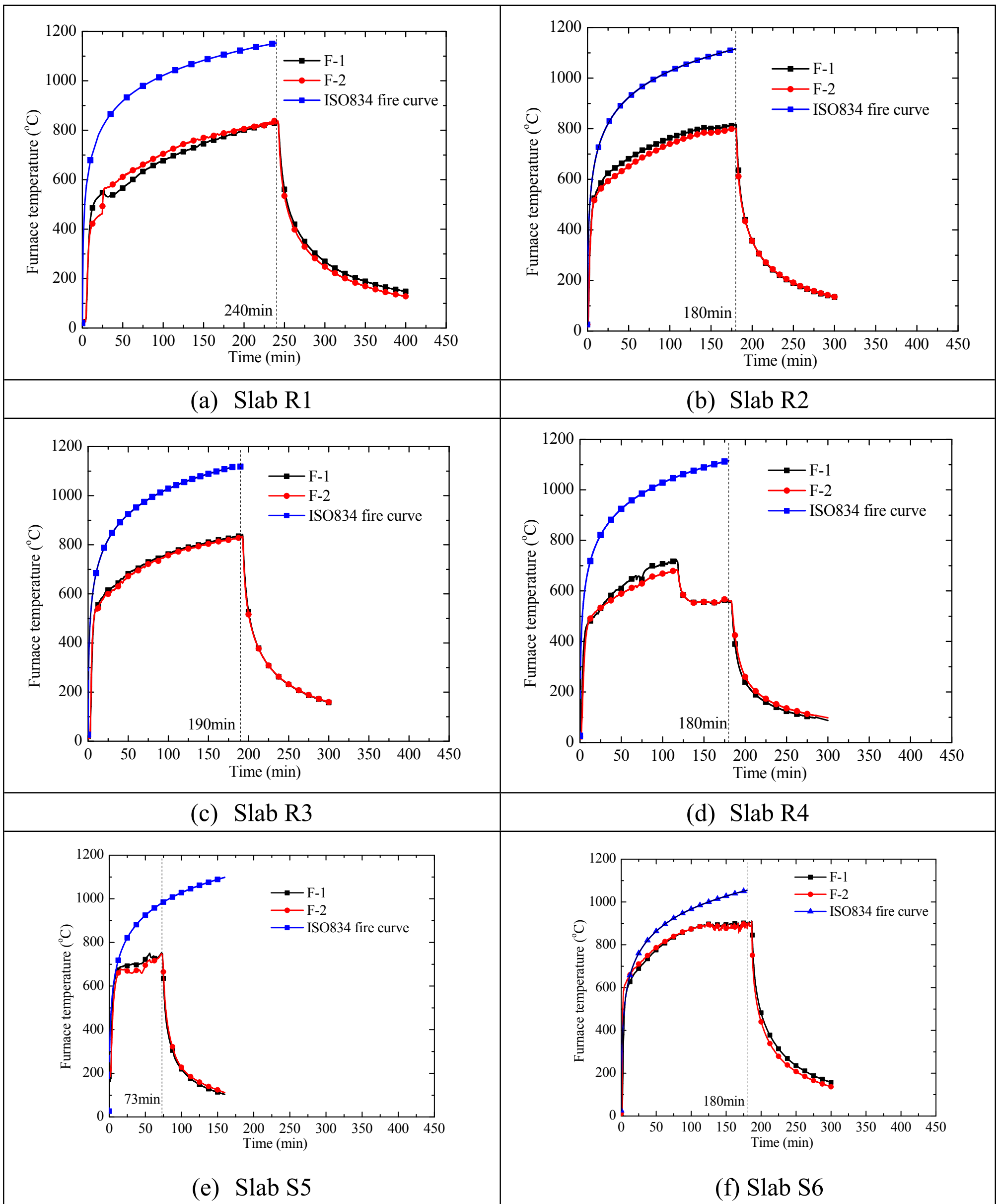

(a) Slab R1
(b) Slab R2
(c) Slab R3
(d) Slab R4
(e) Slab S5
(f) Slab S6

Fig. 5. Furnace temperature-time curves of: (a) Slab R1, (b) Slab R2, (c) Slab R3, (d) Slab R4, (e) Slab S5 and (f) Slab S6.

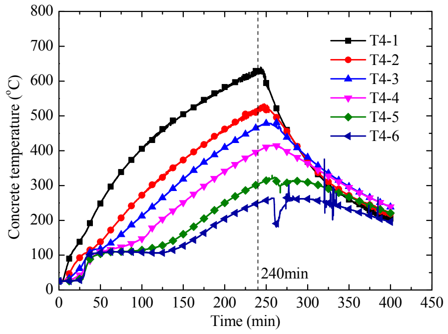

(a) Slab R1

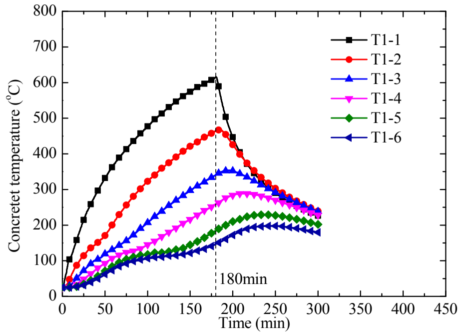

(b) Slab R2

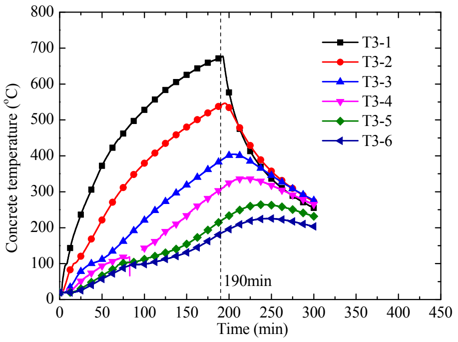

(c) Slab R3

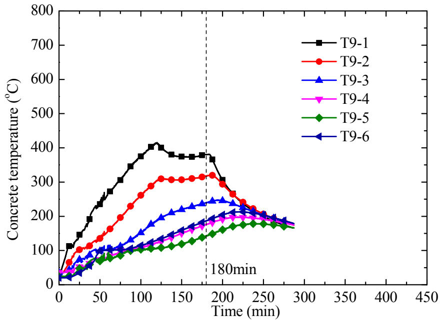

(d) Slab R4

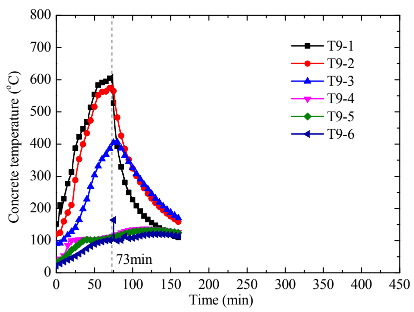

(e) Slab S5

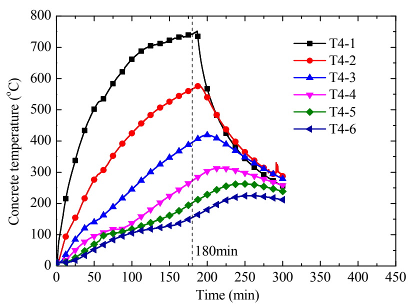

(f) Slab S6

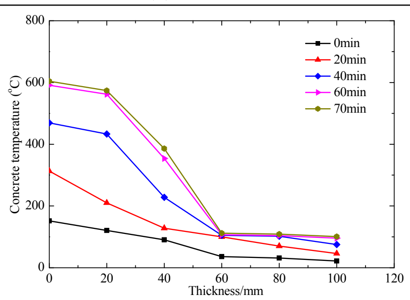

(g) Temperature-thickness in slab S5

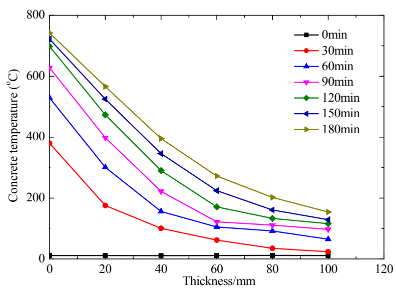

(h) Temperature-thickness in slab S6

Fig. 6. Concrete temperature-time curves of: (a) Slab R1, (b) Slab R2, (c) Slab R3, (d) Slab R4, (e) Slab S5, (f) Slab S6, (g) temperature-thickness curves in Slab S5 and (h) Slab S6

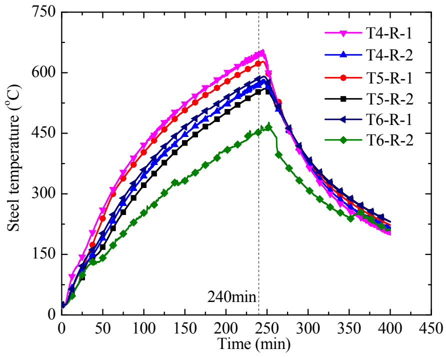

(a) Slab R1

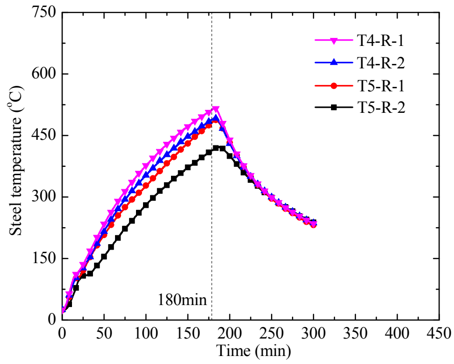

(b) Slab R2

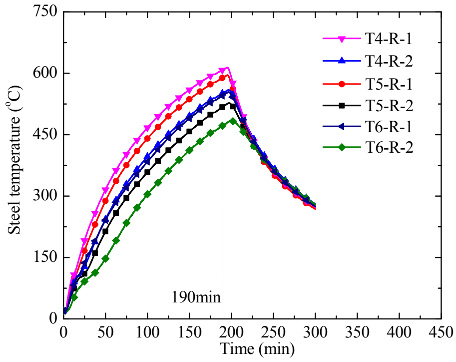

(c) Slab R3

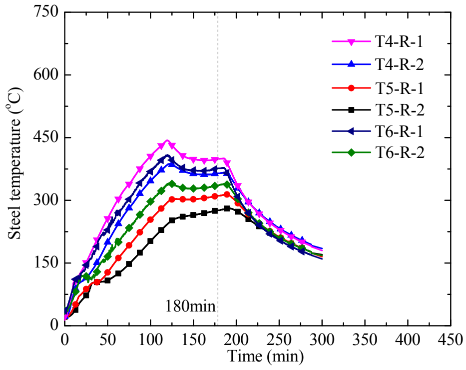

(d) Slab R4

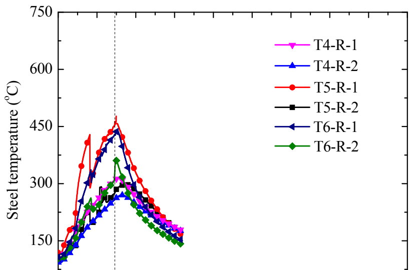

(e) Slab S5

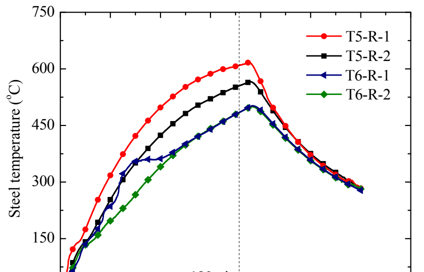

(f) Slab S6

Fig. 7. Temperatures of the reinforcing steels of: (a) Slab R1, (b) Slab R2, (c) Slab R3, (d) Slab R4, (e) Slab S5 and (f) Slab S6.

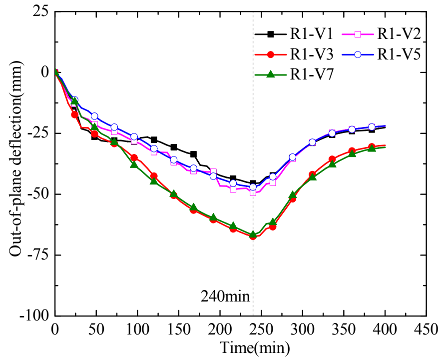

(a) Slab R1

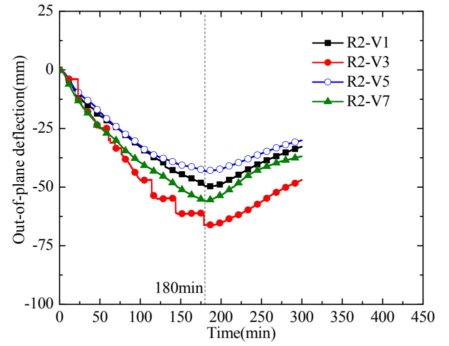

(b) Slab R2

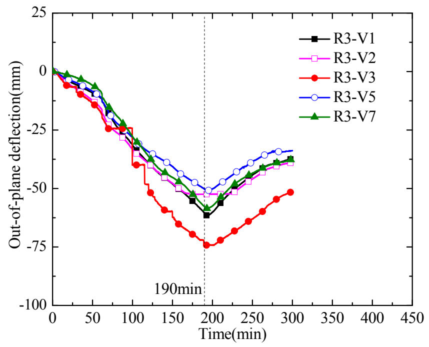

(c) Slab R3

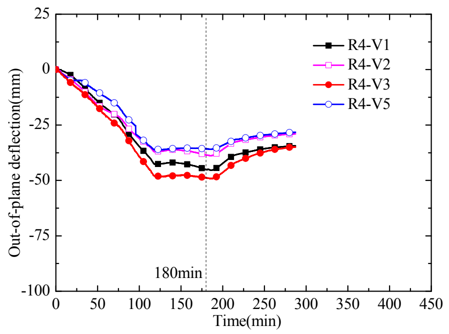

(d) Slab R4

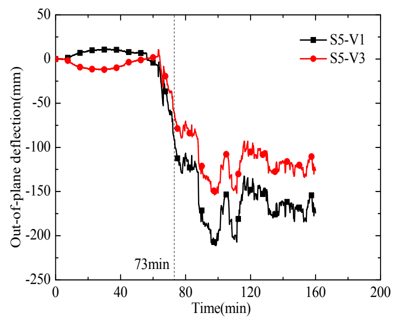

(e) Slab S5

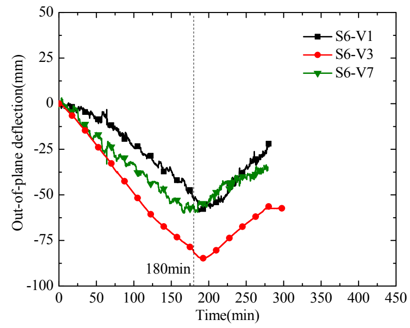

(f) Slab S6

Fig. 8. Vertical out-of-plane deflections-time curves of the Slabs: (a) Slab R1, (b) Slab R2, (c) Slab R3, (d) Slab R4, (e) Slab S5 and (f) Slab S6.

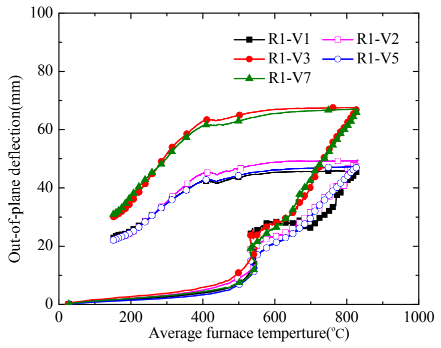

(a) Slab R1

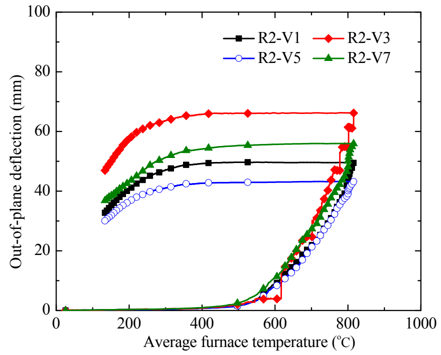

(b) Slab R2

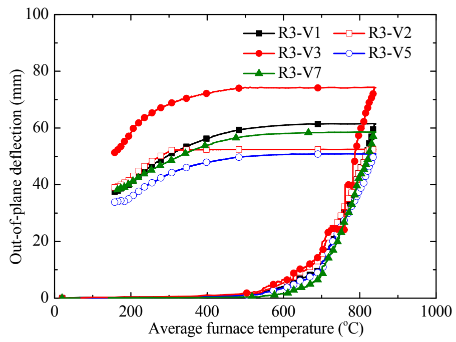

(c) Slab R3

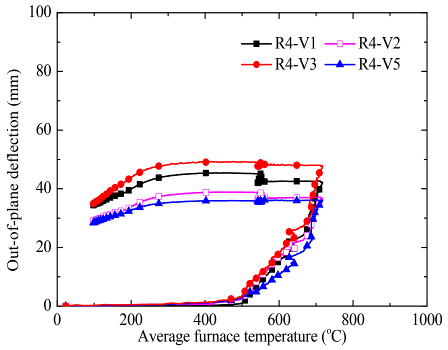

(d) Slab R4

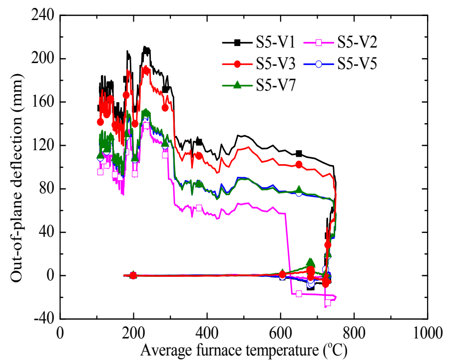

(e) Slab S5

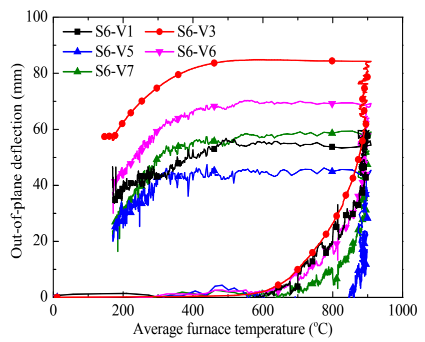

(f) Slab S6

Fig. 9. Out-of-plane deflections-average furnace temperature curves of the slabs: (a) Slab R1, (b) Slab R2, (c) Slab R3, (d) Slab R4, (e) Slab S5 and (f) Slab S6

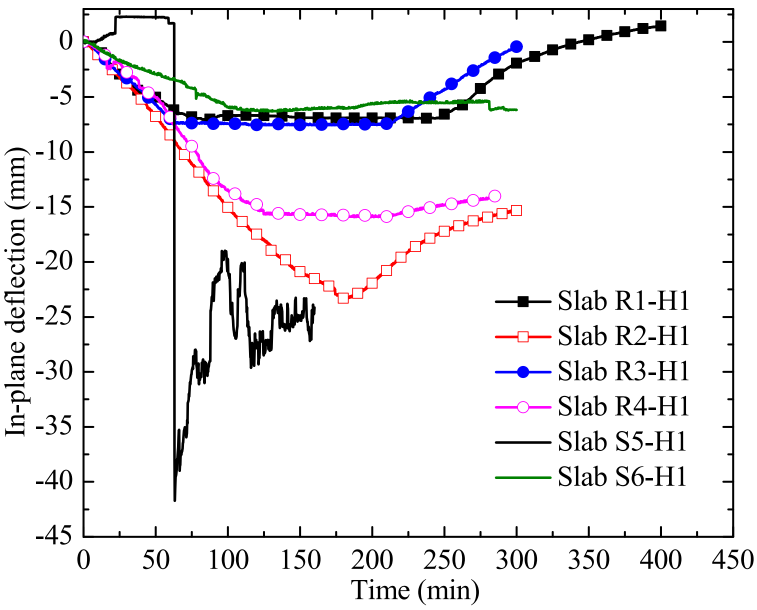

Fig. 10. Horizontal deflections of six concrete slabs

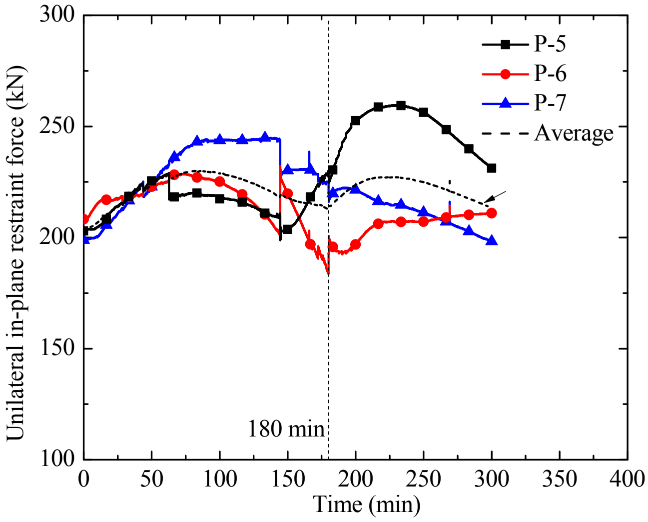

Fig. 11. Measured uni-axial in-plane restraint forces in Slab R2 (N-S direction)

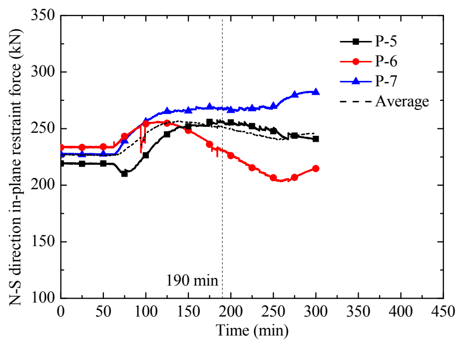

(a) N-S direction

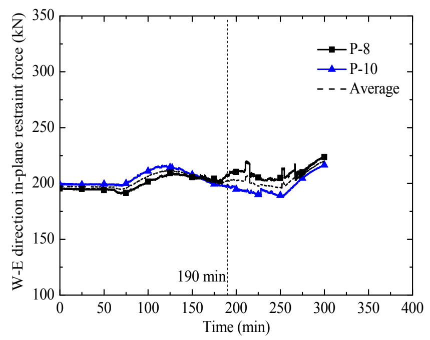

(b) W-E direction

Fig. 12. Measured two directions' in-plane restraint forces in Slab R3

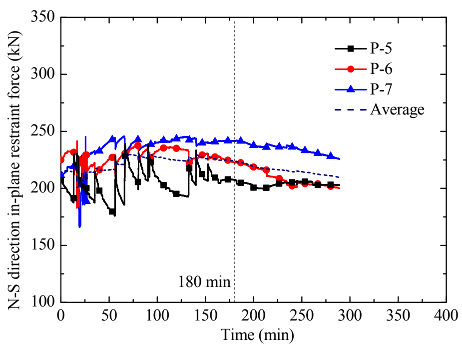

(a) N-S direction

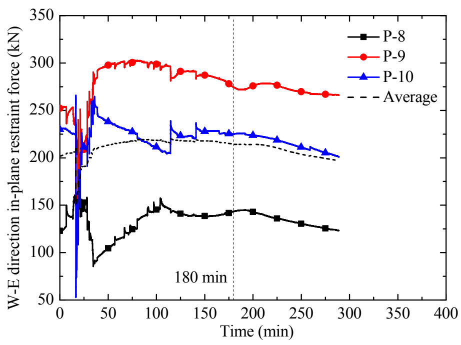

(b) W-E direction

Fig. 13. Measured two directions' in-plane restraint forces in the Slab R4

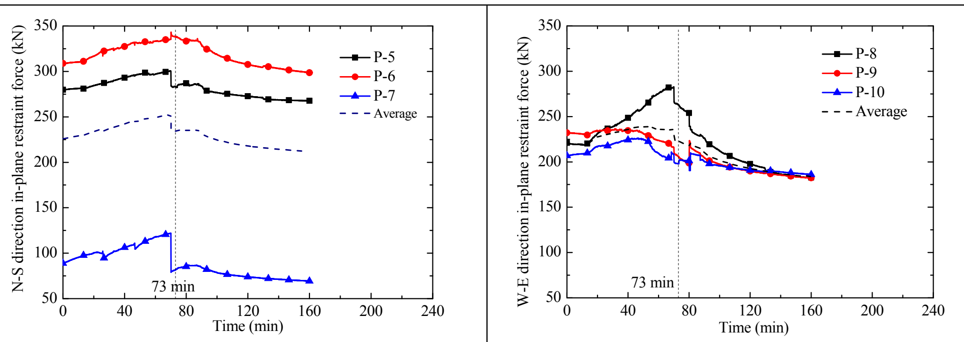

(a) N-S direction (b) W-E direction

Fig. 14. Measured two directions' in-plane restraint forces in Slab S5

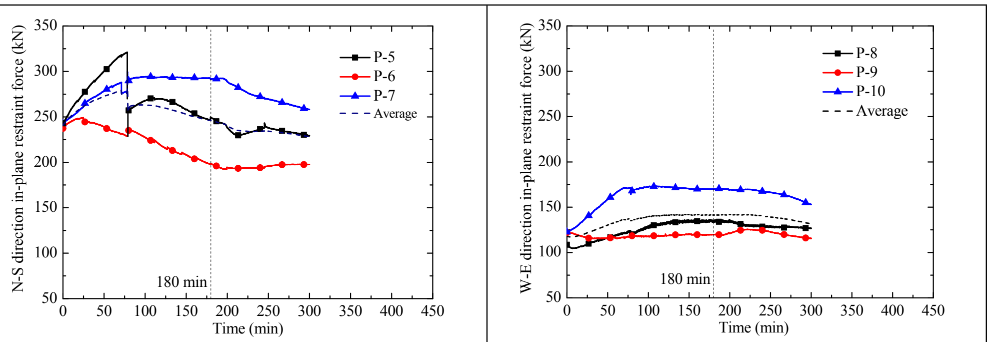

(a) N-S direction | (b) W-E direction

Fig. 15. Measured two directions' in-plane restraint forces in Slab S6

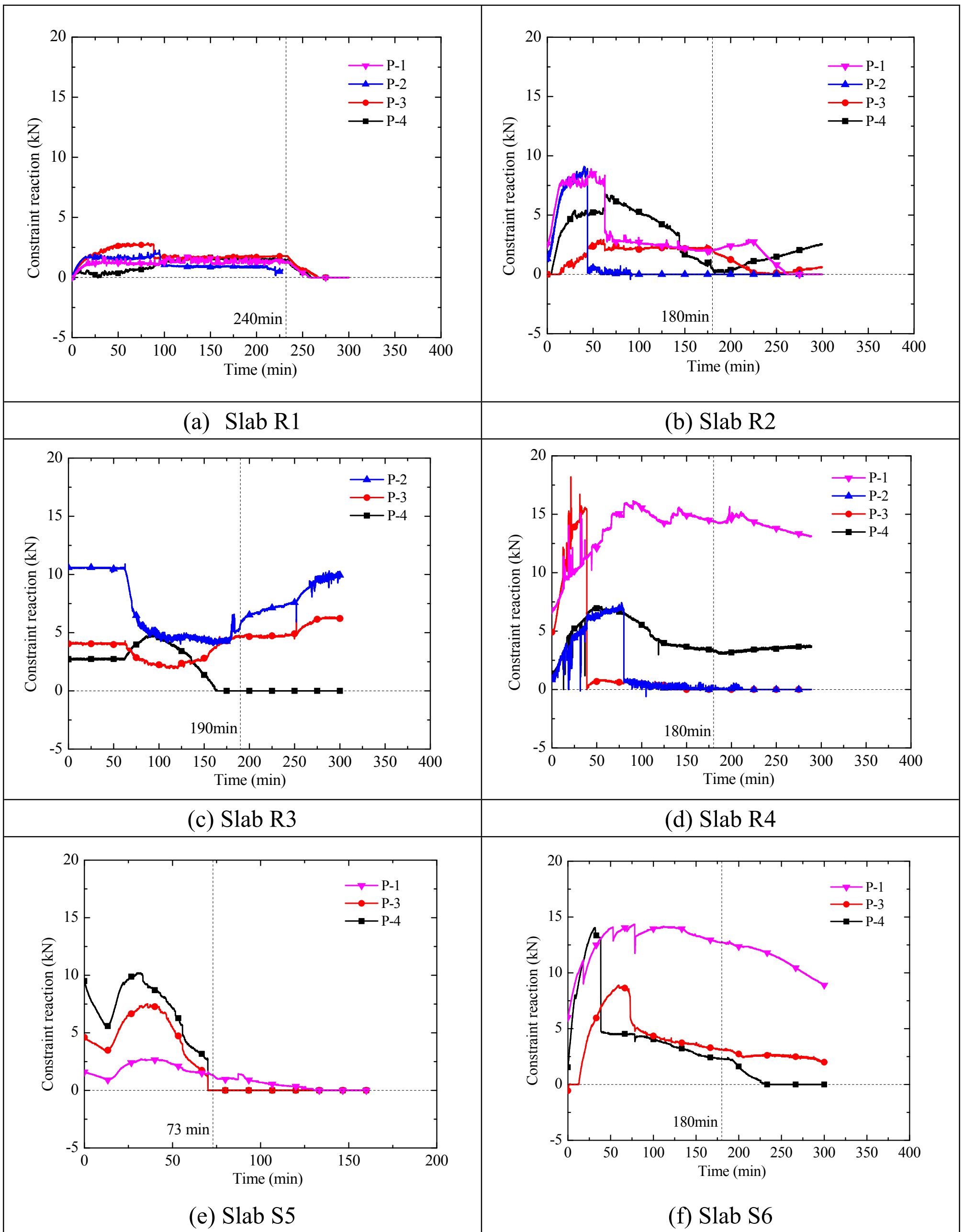

(a) Slab R1
(b) Slab R2
(c) Slab R3
(d) Slab R4
(e) Slab S5
(f) Slab S6

Fig. 16. Restrained forces at the corners of the slabs: (a) Slab R1, (b) Slab R2, (c) Slab R3, (d) Slab R4, (e) Slab S5 and (f) Slab S6

(a) cracking pattern on the top surface

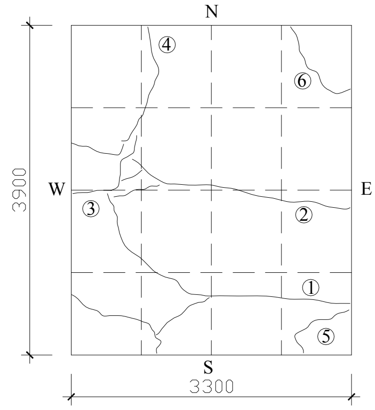

(b) cracks' development during the test

(c) spalling on the bottom surface

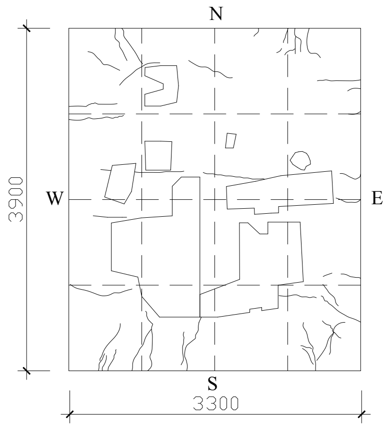

(d) cracking patter on the bottom surface

Fig. 17. Failure modes of Slab R1: (a) cracking pattern on the top surface, (b) cracks' development, (c) spalling and (d) cracking patter on the bottom surface

(a) cracking pattern on the top surface

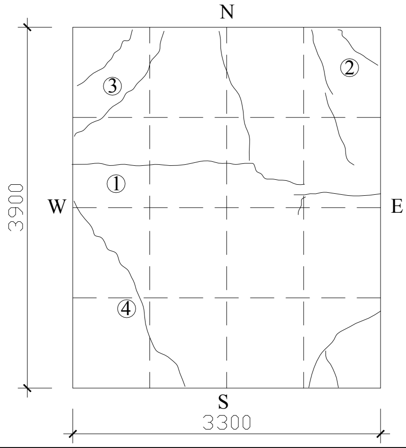

(b) cracks' development during the test

(c) spalling on the bottom surface

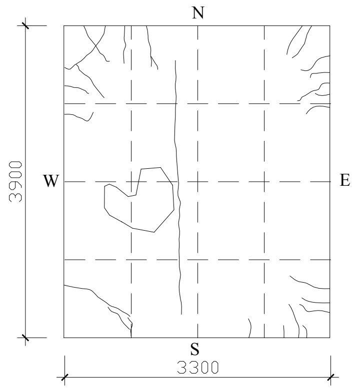

(d) cracking patter on the bottom surface

Fig. 18. Failure modes of Slab R2: (a) cracking pattern on the top surface, (b) cracks' development, (c) spalling and (d) cracking patter on the bottom surface

(a) cracking pattern on the top surface

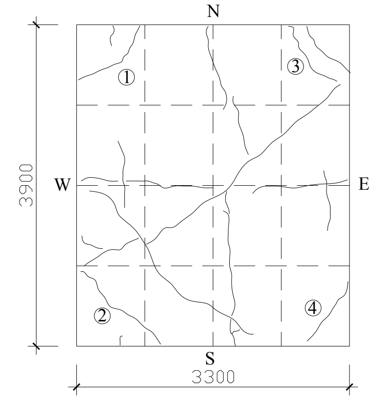

(b) cracks' development during the test

(c) spalling on the bottom surface

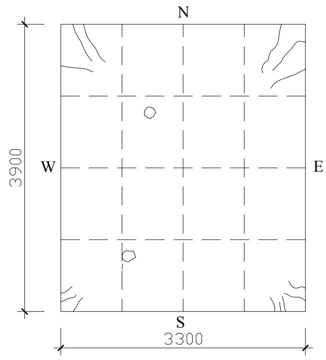

(d) cracking patter on the bottom surface

Fig. 19. Failure models of Slab R3: (a) cracking pattern on the top surface, (b) cracks' development, (c) spalling and (d) cracking patter on the bottom surface

(a) cracking pattern on the top surface

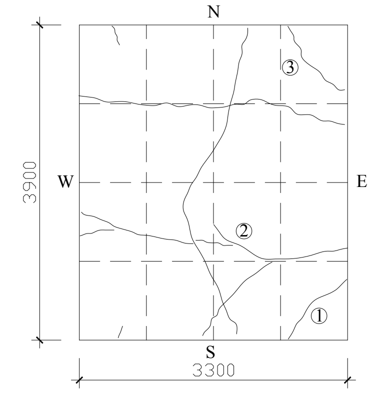

(b) cracks' development during the test

(c) spalling on the bottom surface

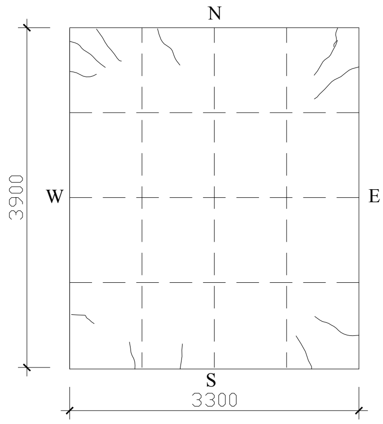

(d) cracking patter on the bottom surface

Fig. 20. Failure modes of Slab R4: (a) cracking pattern on the top surface, (b) cracks' development, (c) spalling and (d) cracking patter on the bottom surface

(a) cracking pattern on the top surface

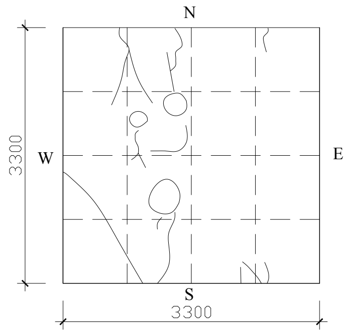

(b) cracks' development during the test

(c) spalling on the bottom surface

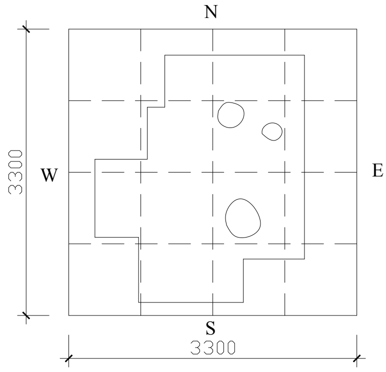

(d) cracking patter on the bottom surface

Fig. 21. Failure modes of Slab S5: (a) cracking pattern on the top surface, (b) cracks' development, (c) spalling and (d) cracking patter on the bottom surface

(a) cracking pattern on the top surface

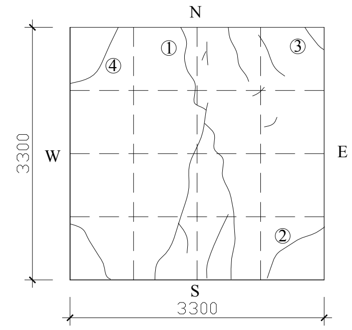

(b) cracks' development during the test

(c) spalling on the bottom surface

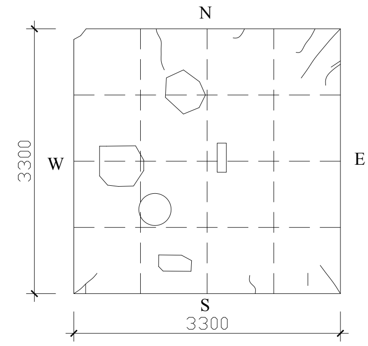

(d) cracking patter on the bottom surface

Fig. 22. Failure modes of Slab S6: (a) cracking pattern on the top surface, (b) cracks' development, (c) spalling and (d) cracking patter on the bottom surface

Tables:

Table 1 Dimensions and applied stress level of six concrete slabs

Slab	L_x	L_y	h	σ_x (MPa)	σ_y (MPa)
R1	3900	3300	100	0	0
R2	3900	3300	100	2.0	0
R3	3900	3300	100	2.0	1.0
R4	3900	3300	100	2.0	2.0
S5	3300	3300	100	2.0	2.0
S6	3300	3300	100	2.0	1.0

Table 2 Average furnace temperatures of six concrete slabs (0~180min) (^{o}C)

t (min)	0	1	3	5	7	10	15	20	30	40	50	60	70	80	90	100	110	120	130	140	150	160	170	180
R1	25	25	25	79	276	418	472	492	550	565	588	613	634	657	674	690	707	721	734	746	757	767	776	786
R2	26	60	323	442	501	538	568	591	620	643	666	687	705	722	737	752	764	774	784	791	792	797	802	809
R3	20	20	76	373	489	539	568	592	620	651	677	700	714	733	747	759	772	784	791	799	807	814	820	826
R4	23	27	201	360	432	473	498	516	550	580	599	624	638	663	677	688	696	642	566	551	556	553	558	559
S5	184	170	309	555	622	657	686	692	698	698	721	732	741	410	277	219	183	158	139	125	113	104	_	_
S6	11	12	438	559	598	626	659	681	716	751	781	806	828	846	862	873	883	888	891	876	886	886	877	888

Table 3 Average furnace temperatures of six concrete slabs (182~400min) (°C)

t (min)	182	185	190	195	200	210	220	230	240	250	260	270	280	290	300	310	320	330	340	350	360	370	380	400
R1	788	791	794	798	803	810	817	827	829	548	429	364	318	285	259	237	218	203	190	179	168	159	151	138
R2	695	563	460	399	356	298	259	230	208	190	175	163	152	143	134	_	_	_	_	_	_	_	_	_
R3	829	830	833	677	522	398	332	288	256	231	211	195	181	169	158	_	_	_	_	_	_	_	_	_
R4	557	488	353	287	249	204	176	157	142	129	120	112	104	102	100	_	_	_	_	_	_	_	_	_
S5	_																							
S6	903	895	650	530	461	374	319	277	246	222	202	185	171	158	147	_	_	_	_	_	_	_	_	_

Table 4 Fire resistance of the restraint concrete slabs based on the different failure criteria (min)

Slab	R1	R2	R3	R4	S5	S6
Rebar temperature	199	No failure	175	No failure	No failure	155
Concrete temperature	173	No failure	188	No failure	No failure	176
Deflection (l/30)	No failure	No failure	No failure	No failure	No failure	No failure
Deflection (l/20)	No failure	No failure	No failure	No failure	No failure	No failure
Rate of deflection	No failure	No failure	No failure	No failure	73	No failure
Heating time	240	180	190	180	73	180